Chalmers University of Technology

KBTX12

Robust, passive and active chemical sampling system for airborne fission products

June 22, 2021

Author:
Ericsson Fredrik
freeric@student.chalmers.se

Supervisors:
Retegan Vollmer Teodora
tretegan@chalmers.se

Foreman Mark
foreman@chalmers.se

Arellano Santiago
santiago.arellano@chalmers.se

Examinator:
Ekberg Christian
che@chalmers.se

Abstract

When an NPP (Nuclear Power Plant) accident happens, fission products are released into the atmosphere, ^{131}I being one of the most prominent of these. To make an informed first response to such a situation, it is of interest to carry out measurements to find out what radionuclides were released and in what quantity. Similarly to a volcanic eruption, an NPP accident can send debris several kilometers up in the air at very high temperatures. UAVs (Unmanned Aerial Vehicles) have been used in previous research for sampling gases in volcanic gas plumes. The aim of this thesis is to provide a proof of this concept for sampling radionuclides. A system for passive and active chemical sampling of radioactive iodine that is intended to be implemented in a UAV is formulated in this thesis. This system consists of the Kromek GR1 γ-ray spectrometer, a pump and two kinds of filters, one containing DABCO-loaded charcoal for capturing methyl iodide, and one containing copper granules for capturing elemental iodine. Cylindrical plastic beads measuring 9 mm in diameter were used as filter cartridges and these were sealed with either fabric or glass fibre sheets. The manufacturing of the filters, and the experiments that were conducted to investigate the filters' ability to capture methyl iodide are described in this thesis. The experiments were carried out both with non-radioactive methyl iodide and methyl iodide containing ^{131}I. The results indicated that the filters were suitable for the purpose, and it was shown that a glass fibre sheet on the outermost filter of the filter tube provided protection against moisture entering the filters. The Kromek GR1 was included in the concept of the sampling system as a device to "sniff out" hotspots of radioactivity. The total weight of the components of the system is 119 g, which is well under the UAV's payload limitation of 2kg, and their total power consumption is less than 1 W. A drone flight to test the sampling system has yet to be conducted. For future research, the concept needs to be tested in a more practical way, by conducting UAV flights and addressing issues such as the robustness of the sampling system. Additionally, the concept can be tried using filters made for sampling other radionuclides than ^{131}I, such as ^{137}Cs.

Contents

1 Introduction

1.1 Background

When serious accidents in NPPs (nuclear power plants) occur, their consequences are often difficult to predict. The causes of these accidents can vary: In the Chernobyl disaster in 1986 it was flawed reactor design and personnel making mistakes.[1] The management of the Chernobyl NPP wanted to conduct an experiment to investigate the possibility of having the generator turbine power the cooling water pumps in case of a power failure. The experiment was poorly planned and the personnel were aware that they were not acting in accordance to safety regulations.[2] This led to an uncontrolled increase in fission rate and reactor power, and caused a RIA (reactivity initiated accident).[3] The resulting explosion sent radioactive matter several kilometers up in the air.[4]. Volatile radionuclides that were reportedly released are Xe, Kr, I, Te, and Cs. Particularly large amounts of ^{131}I, ^{134}Cs and ^{137}Cs were released.[5]
In 2011, the Fukushima NPP was struck by earthquake-induced tsunami waves. The earthquake caused power failure in the electricity network, so diesel generators were started to generate electricity for the cooling system of the NPP. Once the waves were high enough to overcome the 5,7m tall sea-wall, the generators were flooded and could not operate. The waves were ranging up to 14m in height. This led to a LOCA (Loss of cooling accident), which caused meltdown in the reactor core.[6] As a result of this, radioactive nuclides were released from the NPP. In the months following the Fukushima accident, radionuclides in the ocean were sampled by collecting 2 litre samples at the cooling water intake of the power plant. This data was used to study the distribution of radionuclides in the ocean.[7] This project aims to have a sampling system developed, for air instead of water. Therefore, the radionuclides need to be captured in a filter system.
In order to take suitable measures in a nuclear power plant accident scenario, it is useful to be able to analyse the area around the plant without taking the risk of sending human personnel there, as it is not a safe course of action. Knowing what volatile radioactive species are present and in what amounts can help when making decisions on the first response to a nuclear disaster. UAV (Unmanned Aerial Vehicle) application for supporting disaster management has proven to be a successful concept in several different situations not only related to nuclear danger [8] and it is not overly expensive [9]. The main idea of this project is to develop a small chemical sampling system and attach it to a UAV that can be sent into areas badly affected by a nuclear disaster. The sampling system developed has to satisfy the weight constraints that a UAV comes with. Santiago Arellano, who is a researcher, Department of Space, Earth and Environment, Microwave and Optical Remote Sensing at Chalmers University of Technology, and his research team, have used their UAV "Munin" to conduct measurements of gases in volcanic plumes.[10] Similarly to a volcanic eruption, the Chernobyl accident sent radioactive debris several kilometers up in the air at very high temperatures.

2 Purpose

Information being available shortly after an accident can potentially be of vast significance. The purpose of the sampling system attached to a UAV (Unmanned Aerial Vehicle) is to quickly gather information about which volatile radioactive compounds are present in the vicinity of the nuclear plant and in what concentration. If this type of information is available at an early stage, suitable measures can be taken more quickly, which can potentially minimize the negative impact of the accident. A UAV can fly through dangerous areas and measure the air concentration of dangerous isotopes without having to send human personnel into the dangerous area.

2.1 Scope

The design of the aforementioned UAV encompass the design of several different components that must work efficiently when integrated in the system. This thesis focuses on the chemical sampling techniques that will be used to capture iodine particles, and the synthesis of chemical trap particles will also be touched upon. Other issues, such as the operation of the UAV and its spatial location tracking accuracy will not be studied in this thesis but will rather be treated as a sidenote. The sampling system will be implemented in the UAV. The sampling system developed in this project should be considered not as a sampling system for all volatile radioactive species, but rather as a proof of concept for flying a UAV with a chemical sampling system. The filters will primarily be designed to capture iodine and methyl iodide. Making filters specifically designed to sample other volatile radioactive species will be left for future studies. Charcoal-based filters [11] will be the primary test subject for the sampling filters. Nonporous pillar[6]arene crystals [12], and hexaphenylbenzene-based conjugated microporous polymers [13] would also be potential options for capturing iodine but these will not be looked at in this project. The filter system that is developed in this project is inspired by the May-pack, which is an iodine sampling system that consists of a series of different filters that capture different volatile radioactive iodine compounds.[14] Volatile organic iodine compounds of interest to be captured are methyl iodide (CH_3I) ethyl iodide (C_2H_5I), isopropyl iodide ($(CH_3)_2CHI$), chloromethyl iodide (CH_2ClI) and iodidoacetylene (C_2HI).[15]

In this project, methyl iodide and $^{131}I_2$ will be focused on. An article published shortly after the Chernobyl accident investigates the formation of volatile organic iodine compounds. In these experiments, a gas stream of various hydrocarbons were introduced a reaction vessel containing iodine in water solution. The results indicated that methyl iodide was the only organic iodine compound that was being formed in detectable amounts.[16] Methyl iodide reportedly has an atmospheric lifetime of 13.59 days at mid latitudes.[17] Because of the long life-time of methyl iodide in air, it can spread far after being released into the atmosphere.

3 Theory

3.1 Fission product release from nuclear accidents

As discussed in the introduction section, different fission products can be released from an NPP accident. Ratios between certain different radionuclides can be used to yield information about an event where radionuclides were released. For example, if ratio of ^{135}Cs and ^{137}Cs in the environment surrounding a an accident-struck nuclear reactor closely matches that of the reactor, the radionuclide release can be traced to that reactor.[18] Fission products released from the Chernobyl accident were transported with the wind and spread over a large portion of the northern hemisphere.[19] Among the radionuclides released from the Chernobyl accident were ^{95}Zr, ^{95}Nb, ^{103}Ru, ^{106}Ru, ^{106}Rh, ^{125}Sb, ^{129m}Te, ^{134}Cs, ^{137}Cs, ^{140}Ba, ^{140}La, ^{141}Ce and ^{144}Ce. After dust samples were collected in the region of Thessaloniki, Greece in June and July 1986, it was reported that ^{131}I constituted about a third of the activity in the fallout.[20] It has been estimated that $1.7 * 10^{18}$ Bq of ^{131}I was released as a result of the Chernobyl accident.[21] As for the Fukushima accident, it has been estimated that $1.5 * 10^{17}$ Bq of ^{131}I and $1.3 * 10^{16}$ Bq of ^{137}Cs were released.[22]

3.2 Radioactive iodine (^{131}I)

^{131}I is a short-lived isotope, its half-life being 8.02 days.[23] ^{131}I decays into Xenon and emits β and γ radiation.[23] The decay scheme of ^{131}I, which is shown in figure 1 shows the types of radiation and their respective energies emitted in the different decay modes. The energies of the γ-rays become important in the HPGe detector analysis which is described later in the method section. In the aftermath of the Chernobyl accident, it was observed that the release of ^{131}I has the potential to have hazardous impact on thyroids of children within a distance of 300 miles from the nuclear site.[24] 10–30 % of ingested radioactive iodine accumulates in the thyroid [25]. However, the health hazards of ^{131}I has been subject to debate. LE Holm argues that a significant portion of the children that developed thyroid cancer were living in iodine-deficient areas. He reasons that this is an indication that children living in iodine deficient areas are much more prone to developing thyroid cancer than children living in less iodine-deficient areas, rather than an indication of ^{131}I being dangerous.[26] ^{131}I is commonly used for treatment of thyroid cancer for adults. Since it accumulates in the thyroid, it is a way of targeting thyroid tumors.[27] After the Chernobyl disaster, it was reported the emergency workers ate iodine pills in order to prevent accumulation of ^{131}I in the thyroid.[28].

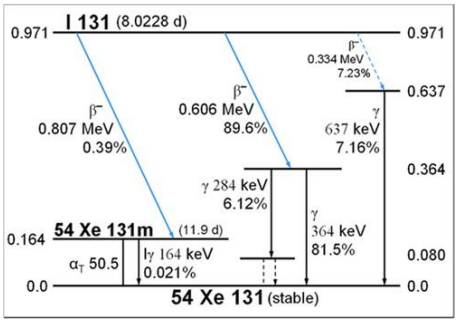

Figure 1: The decay scheme of ^{131}I. [23]

In nuclear disaster scenarios, radioactive iodine commonly occurs as two volatile species: Elemental iodine and CH_3I (methyl iodide). Two ways of methyl iodide forming as a result of nuclear power plant accidents were proposed by Beahm *et al.*[16] Methyl radicals and iodine radicals are formed by reactions involving the $OH\bullet$ radical, see reactions 3 and 4. These radicals then combine in reaction 7 to form methyl iodide. The $OH\bullet$ radical is formed by ionizing radiation causing radiolysis of water, see reactions 1 and 2.[29] ^{131}I for experimental use can be manufactured by exposing tellerium oxide, TeO_2, to neutron radiation, forming ^{131}I according to reaction 8.[30]

$$H_2O \rightarrow H_2O^+ + e^- \tag{1}$$

$$H_2O^+ + H_2O \rightarrow H_3O^+ + OH\bullet \tag{2}$$

$$OH\bullet + I^- \rightarrow I\bullet + OH^- \tag{3}$$

$$OH\bullet + CH_4 \rightarrow CH_3\bullet + OH^- \tag{4}$$

$$I\bullet + CH_3\bullet \rightarrow CH_3I \tag{5}$$

$$I\bullet + I\bullet \rightarrow I_2 \tag{6}$$

$$I_2 + CH_3\bullet \rightarrow CH_3I + I\bullet \tag{7}$$

$$^{130}_{52}Te + ^{1}_{0}n \rightarrow ^{131}_{52}Te + \gamma \rightarrow ^{131}_{53}I + ^{0}_{-1}e + \gamma \tag{8}$$

Radioactive methyl iodide, which was mentioned earlier as one of the most common iodine compounds formed in NPP accidents, can be produced by dissolving the ^{131}I in a potassium iodide solution and having it react with dimethyl sulfate ($(CH_3)_2SO_4$), see reaction 9. For this method, an 88 % radiochemical yield is reported by Tietze *et al.* The synthesized methyl iodide is then stored cold, in liquid phase. Because of its volatility, it can easily be converted between liquid and gas phase according to what the planned experiments require.[31]

$$(CH_3)_2SO_4 + KI \leftrightarrow CH_3I + KSO_3(OCH_3) \tag{9}$$

3.2.1 Chemical mechanisms for iodine capture

CuI has been suggested as a final wasteform for ^{129}I by Vance *et al.* [32] ^{129}I is a long-lived isotope, unlike ^{131}I. However the strong chemical affinity between copper, which is one of the main reasons for the suggestion, also makes copper useful for capturing elemental ^{131}I. In 1961, an iodine sampling device was developed by May and Megaw.[33] This later came to be known as the "May-pack". The May-pack is an iodine sampling system that consists of a series of different filters that capture different volatile radioactive iodine compounds. A schematic drawing of the May-pack is shown in figure 2. The blue lines represent charcoal impregnated paper filters, and the dashed black line represents a millipore filter and the dashed red lines represent silver coated copper gauzes. These components not only capture iodine-containing compounds, they also separate different iodine-containing species. Elemental iodine is captured on the copper gauzes and the charcoal impregnated paper filters, the millipore filter prevents large particles from passing through it. The charcoal pads (on the left of figure 2) capture compounds containing iodine.[34] Historically, charcoal impregnated with different compounds have been used for capturing methyl iodide. For example, in 1971, charcoal impregnated with stannous iodide or potassium thiocyanate have were reported to efficiently capture methyl iodide, and with DABCO-loaded charcoal, it was reported that the 98% of the methyl iodide radioactivity was captured, despite high humidity conditions.[35] Not being negatively affected by weather conditions is a desirable property of a sampling system which is to be fitted on an UAV. Another advantage of DABCO-loaded charcoal is that it is easily available, as it can be found in respirator filters. DABCO captures CH_3I molecules by a nucleophile attack by the tertiary amine group nitrogen atom on the sp^3 carbon in the methyl iodide molecule. The iodine atom acts as the leaving

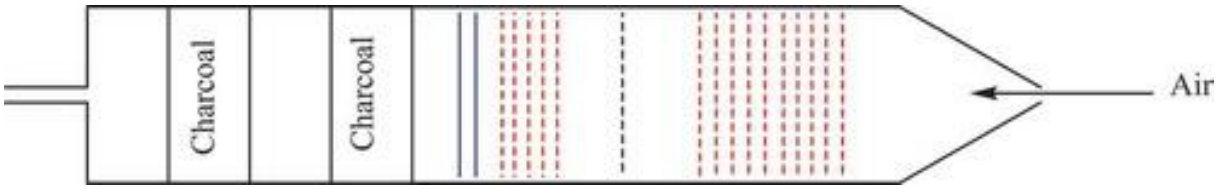

Figure 2: A schematic drawing of the May-pack.[34]

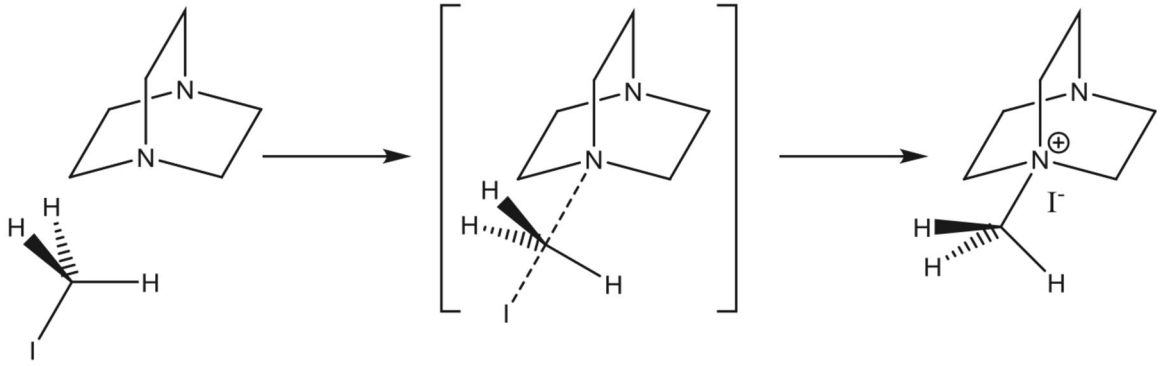

Figure 3: An illustration of the S_N2 reaction mechanism through which DABCO captures CH_3I.[15]

group and takes with it the electron pair, thus becoming a negatively charged ion and leaving a polyatomic cation. This is illustrated in figure 3. The strong ionic bond is what constitutes the strong chemical affinity between DABCO and CH_3I. The nitrogen atoms in DABCO also have the ability to bind to copper, and if they do, they cannot capture any methyl iodide, and the efficiency of the filters is reduced. Thus, the DABCO and the copper should be kept in separate filters cartridges.[15]

3.3 Pump specifications

Passive sampling means that there is no pump sucking air through the filters. For the active sampling experiments, there needs to be a pump that sucks in air through the filters. Two RS PRO Diaphragm Electric Operated Positive Displacement Pumps were ordered from RS, see figure 4. The specifications provided by the supplier are tabulated in table 1. It's weight was measured to be 45 g. When implementing the system on a UAV, it is desired that the payload weighs as little as possible, as heavier payload means shorter flight time.

Table 1: Specifications for the RS PRO Diaphragm Electric Operated Positive Displacement Pump.

Input connection	2.4 mm
Output connection	2.4 mm
Body	Aluminium
Maximum working pressure	11 psi
Maximum fluid temperature	100°C
Maximum flow rate	380 ml/min
Input power	0.48W
Working voltage range	1.5-5 V

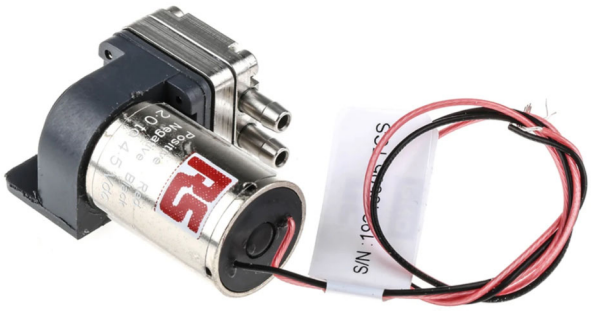

Figure 4: The RS PRO Diaphragm Electric Operated Positive Displacement Pump.

3.3.1 UAV Specifications

The SkyEye innovations micro, shown in figure 5 is the UAV on which the sampling system will be implemented. Its specificatoins provided by the suppliers are shown in table 2. It has the capacity to carry 2 kg of payload. It is important that the sampling system satisfies this constraint, preferably with a great margin. The lighter the payload is, the longer the potential flight time. For the same reason, it is also desirable that the electric power consumption of the components of the sampling system is as low as possible.

Table 2: Specifications for the SkyEye Innovations Micro UAV.[10]

Model	SkyEye Innovations Micro
Nickname	Munin
Configuration	Y6 multi-rotor (three pairs of co-axial, counterrotating rotors in tandem)
Navigation system	PixHawk model V4
Remote control	Jeti DC16
Drone size (D*H*W) / cm	80*20*23
Frame weight, without batteries / kg	3.0
Drone weight, including batteries / kg	4.5 – 6.0
Maximum payload / kg	2.0
Maximum combined thrust/ N	120
Battery voltage / V	22.2 (6*3.7)
Battery capacity / Ah	20 (2*10)
Control range / km	5
Typical flight time (1 kg payload) / min	30
Maximum climb speed / ms^{-1}	5
Maximum descent speed / ms^{-1}	4
Maximum cruise speed (still wind) / ms^{-1}	10

Figure 5: The SkyEye Innovations Micro drone.

3.4 Kromek GR1

The Kromek GR1 is a small USB-powered γ-ray spectrometer. Equipped with a CZT (Cadmium Zinc Telluride)-detector, it can measure the γ-radiation which is emitted from the radionuclides that are close enough to it. The manufacturer claims that the GR1 is "The world's smallest and highest resolution room temperature gamma ray spectrometer".[36] It has been used previously on UAVs for γ-radiation monitoring. Thanks to its size, which can be seen in figures 6 and 7, its weight being 59 g and its power consumption being 250 mW, it is suitable to mount on a UAV. It works in the tempearture range 0-40°C, so avoiding extreme temperatures has to be considered when flying the UAV. [37]

Figure 6: The Kromek GR1 γ-ray spectrometer.

Figure 7: The side of the Kromek GR1 with a socket for a USB cable

3.5 Chemical analysis techniqeus

3.5.1 ICP-OES

Some metals give the flame a characteristic colour when burned, such as sodium, potassium and calcium.[38] Each element has a spectrum of wavelengths specific to it when emitting light due to de-excitation of electrons in an excited state. This can serve as a fingerprint for the element, and this is behind the operation of the ICP-OES (Inductive Plasma Coupling Optical Emission Spectroscopy) machine.[39] ICP-OES is good for measuring elemental concetrations in the range 0-20 ppm and thus it was chosen as the method for measuring concentration of non-radioactive iodine. The sample to be studied is pumped into a nebulizer which sprays the liquid into a hot argon plasma (5000-9000K) which atomizes the sample (that is it breaks all the chemical bonds). The electrons go into an excited state as the is energy absorbed from the plasma. When the electrons go back from the excited state to the ground state, the energy is emitted as quanta of light. Each element emits a specific spectrum of wavelengths, and from this, the elements present can be distinguished from one another.[40] By measuring the intensity of the wavelengths, the amount of each detected element can be determined. It is important to choose a fitting matrix solvent when preparing samples for ICP-OES analysis, in order to avoid matrix effects impacting the measurements. Iodine has been reported to be prone to forming iodates and iodides in acidic solutions, which may cause loss of analyte, carry-over, and memory effects that may impact later measurements.[41] Taking this into account, ammonia was chosen as matrix solvent. Having blank samples

in each batch of samples helps monitoring memory effects.[42] Additionally, having an internal standard is a way of keeping track of matrix effects.[43] IUPAC's definition of an internal standard "A compound added to a sample in known concentration to facilitate the qualitative indentification and/or quantitative determination of the sample components."[44] Cobalt, in the form of $K_3[Co(CN)_6]$, was chosen as the internal standard element when analysing samples for iodine content using the ICP-OES machine.

3.5.2 HPGe detector

Figure 8 depicts a HPGe (High Purity Germanium) detector. It is a semiconductor detector, and it works as follows. The sample vial is placed inside thick lead walls in order to attenuate background radiation. When γ radiation photons emitted by the sample is absorbed by the germanium crystal, free electrons are generated, which generates a voltage. This results in an electric pulse which is then integrated by an amplifier. The amplified signals are registered by a MCA (Multi Channel Analyser) system which displays them as a spectrum, which is a graph where the count rate are plotted against the energy of the incoming γ photons. The tank below the detector in figure 8 contains liquid nitrogen, which keeps the germanium crystal cold in order to minimize the amount of thermally generated charge carriers as these would cause noise in the spectra. The peaks in the spectrum are used to identify what radionuclides are present in the sample. The height of the peaks are proportional to the activity of the corresponding radionuclide present in the sample.[45] The main peak for ^{131}I is at 364,483 eV, which makes up 81,2 % of the γ-radiation energy released during decay.[46] If the rate at which γ-photons are emitted is too high, the detector will not be able to register all of them. The deadtime of the detector is a parameter which quantifies this property. It is defined as the time that it takes for the detector to separate two distinct events from each other. The γ photons emitted within the same deadtime will pile up and register as a count for the sum of their energies. Because of this, samples that have too high activity cause the detector to register counts on energies of γ-photons that are not emitted by the sample.[47] If one would increase the distance from the crystal, lower count rates would be recorded. This can be done by attaching the sample on the wall of the inside of the machine. Another way of handling this, if the nuclide to be measured has a short half-life, is to wait for the activity to decrease and measure later. In order to account for the deadtime of the detector in the calculations, the count rate is determined by dividing the number of counts by the livetime of the detector. The livetime is defined as the difference between the measuring time and the dead time.[48]

Figure 8: A HPGe detector. The sample is placed inside the lead shielding on the top. The tank below contains liquid nitrogen to keep the germanium crystal cold.

4 Method

4.1 Radiation protection

Chalmers' standard radiation protection guidelines instructs all personnel who work with radionuclides to follow the ALARA principle. The acronym ALARA stands for "As low as reasonably achievable" and the principle is to take all possible reasonable measures to minimize exposure to radiation, no matter the dose.[29] Examples of this are minimizing exposure time by planning experiments carefully, keeping all radioactive matter behind thick lead bricks when they are not in use and holding the vial containing radioactive matter for as short time as possible or keeping a distance by holding radioactive samples with tools such as pliers or litter pickers.

4.2 Calculations

A bead sealed with fabric on one side and open on the other was weighed empty and then weighed when it was filled with charcoal in order to determine the amount of charcoal in each filter. Aneheim *et. al* have reported that for charcoal obtained from 3M-respirator replacement cartridges, the amount of DABCO specific to the charcoal was determined to be $346 \mu mol/g$ by elemental analysis. When determined by acid/base titration, it was $381 \pm 6 \mu mol/g$.[15] The weight of the charcoal contained in one filter was weighed to be 0.4069 g. Each DABCO-molecule can bind two CH_3I molecules as it has two tertiary amine groups, see figure 3. It was thus calculated that the DABCO-loaded charcoal in one filter bead could potentially capture up to about 44 mg of CH_3I. The density of CH_3I at room temperature is 2.28, so 44 mg CH_3I corresponds to 19.3 μL of CH_3I.[49] Calculations regarding the results from ICP-OES and γ-ray spectroscopy analysis can be viewed in appendix.

4.3 Experimental preparations

4.3.1 Making the filters

The test filters were made out of cylindrical plastic beads with an outer radius of 9 mm and an inner radius of 6 mm, see figure 9. These were be sealed by a piece of hosiery fabric on each end. The composition of the fabric is 88 % polyamide and 12 % elastane and it was made in Turkey. The fabric was pressed on to one open end of the bead with a soldering machine. The tip of the soldering machine was 200°C hot, so the two would stick together by melting. Then the bead was filled with DABCO-loaded charcoal and sealed on the open end with fabric the same way as the other end before. The filters containing copper granules were made in the same way, sealing the bead with an 8mm glass fibre sheet instead of fabric. Some empty filter cartridges sealed with glass fibre sheets were made too. These were to be used for testing the glass fibre sheets resistance to letting moisture permeate it.

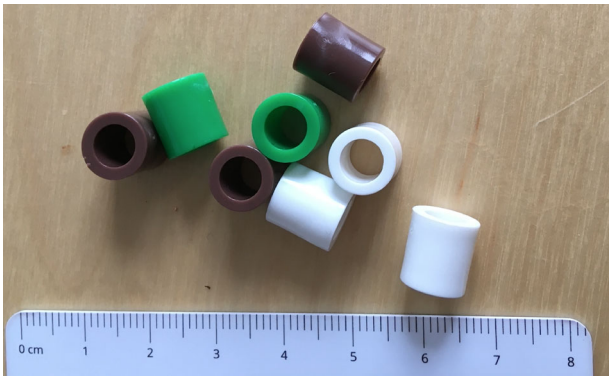

Figure 9: The plastic beads that served as filter cartridges.

Figure 10: A 3M-respirator filter cartridge.

DABCO-loaded charcoal was obtained from a 3M-respitrator filter, see figures 10 and 11. One empty cartridge sealed with a glassfibre sheet, and five charcoal filters were put into PVDF (Polyvinylidene fluoride) shrink tubing and heated. The tube was shrunk using a heat gun, while a 2,4mm plastic tube was inserted into it. Figures 13 through 21 show this process.For the radioactive experiments, one filter containing copper granules and five filters containing DABCO-loaded charcoal (in that particular order) were put into shrink tubing and heated. The filter filled with copper granules was placed as the first filter in order to prevent elemental iodine from entering the Charcoal filters, as these are dedicated for capturing methyl iodide.

4.4 Experimental setup

4.4.1 Passive and active sampling

Both a passive and an active sampling system are intended to be mounted on the UAV. This is because the active filter system might get overloaded with radioactivity. Having a passive one which will give a lesser reading, can facilitate making an accurate assessment on the condition of accident site.

Testing the filters in passive sampling system was carried out as follows. A filter cartridge containing DABCO-activated charcoal was placed in a glass bottle and 2 μL of radioactive methyl iodide was injected into the bottle, using a syringe. The bottle was sealed with a cap for 70 minutes, and then the filters were taken out. In order to measure how much methyl iodide had been caught, the filters were placed in screw top vials and analysed using a HPGe detector. This experiment was repeated three times.

Figure 11: Two opened 3M-respirator filter cartridges from which DABCO-loaded charcoal was obtained.

Figure 12: A plastic bead filled with copper granules, before being sealed on the top.

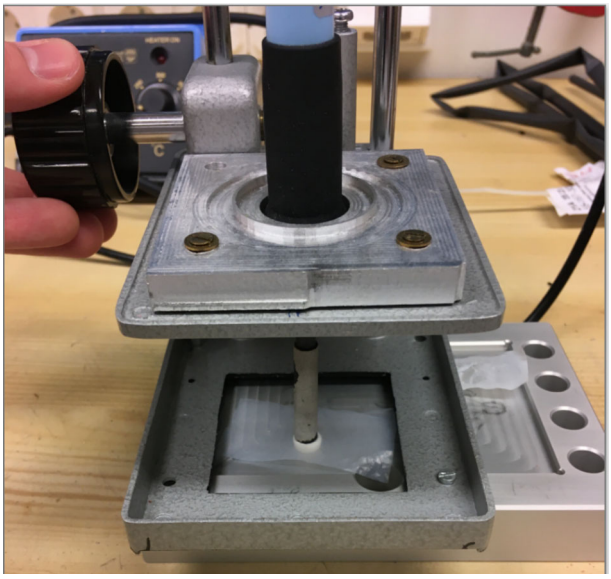

Figure 13: The soldering machine that was used to seal the bead.

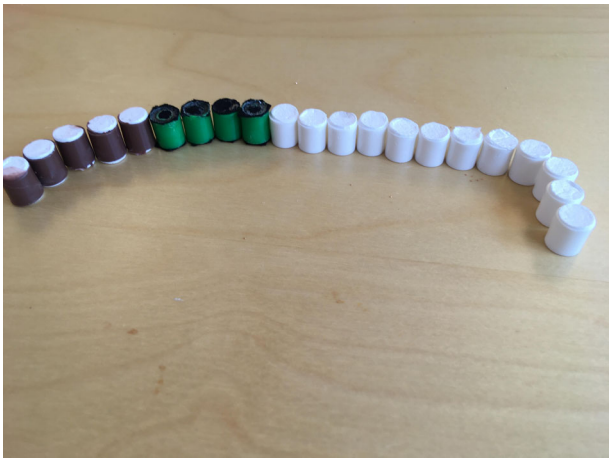

Figure 14: The finished filter cartridges. The green ones contain DABCO-loaded charcoal, the brown ones contain copper granules and the white ones are empty.

Figure 15: The finished filter tubes with plastic tubes connected.

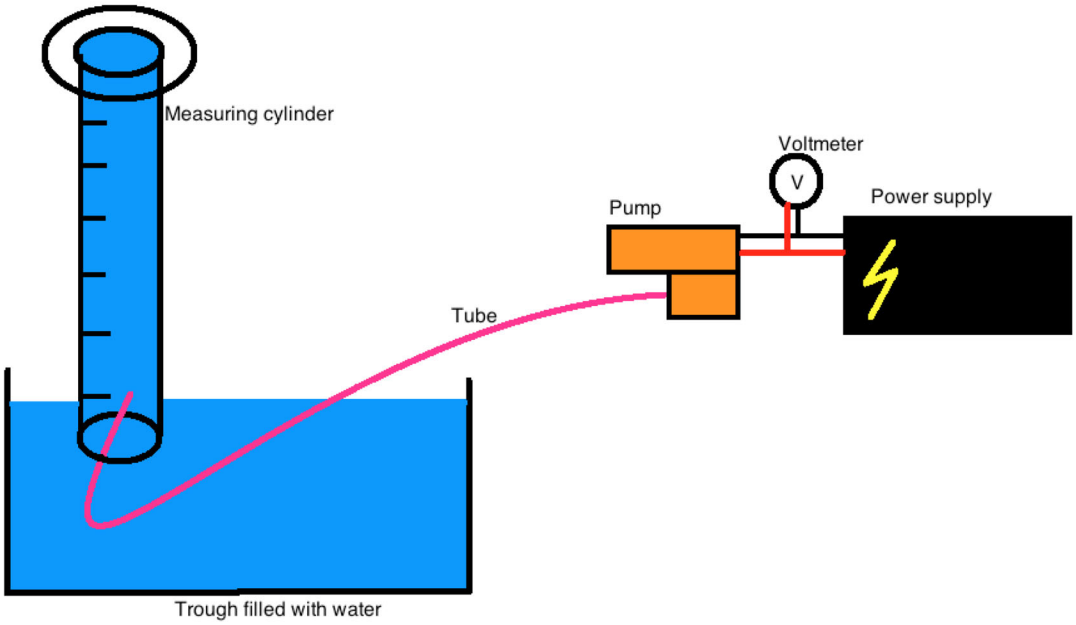

Figure 16: A Schematic drawing of the experimental setup for investigating the flow rate of the pump and its dependence on input voltage.

4.4.2 Pump calibration

For the active sampling system, it is of interest to know at which flow rate the pump is sucking in air through the filters. This was investigated as follows. A measuring cylinder was filled with water and placed upside down in a water bath. A tube connected to the blowing nozzle was inserted into the measuring cylinder. The flow rate of the pump was measured using a stopwatch for three different voltages in the range within which it can operate. A voltmeter was connected to the pump so that it could be monitored during the measurement. The working voltages were set to 2.97, 3.08 and 3.77 V. A linear regression curve was then fitted to these three points. The setup for this experiment is shown in figure 17 and a schematic drawing of it is shown in figure 16.

4.4.3 Glassfibre resistance to sucking in liquid droplets

The experimental setup for this was a cardboard box with two holes poked in it, one for the spray bottle and the other for tube containing empty filter cartridges sealed with glass fibre sheets. Figure 18 shows a schematic drawing of the experimental setup. Flourescein dye was sprayed into the box in order for the RS pump to suck it in through the filter tube. Four experiment runs of 10 minutes were conducted, with 6, 15, 20 and 30 squeezes of the spray bottle handle respectively. The amount of water released by the spray bottle in one squeeze of the handle was measured 23 times and yielded an avarage of 0.45g, and a standard deviation of 0.09g. No dye could permeate the first glass fibre sheet. With this setup, it could thus be shown that the glass fibre sheet would prevent liquid from going through the glassfibre sheet, given the flow rate of the pump did not exceed 500ml/min. This is shown in figure 20. In the following experiments 20μL of methyl iodide is to be injected onto the filter tubes, thus it is of practical importance that no liquid goes through as the filter is meant to sample air.

Figure 17: The setup for carrying out pump flow rate measurement

4.5 Chemical analysis techniques

The samples from the experimental runs using non-radioactive methyl iodide were prepared for and analysed using the ICP-OES machine. The samples from the experimental runs using radioactive methyl iodide were analysed using a HPGe detector. These two analysis techniques are described in the following subsections.

4.5.1 Analysis of non-radioactive iodine, ICP-OES

For the ICP-OES analysis, two matrix solutions were prepared: by diluting a 33% (w/w) ammonia, 50 mL with 450 mL water and 5 mL with 495 mL water respectively. These were denoted solution A and B respectively. Cobalt was used as internal standard element for the ICP-OES analysis. It was added to the solution in the shape of potassium hexacyano coboltate(III) ($K_3[Co(CN)_6]$), up to a concentration of 4 ppm. A stock solution of NaI dissolved in solution B was prepared for the calibration of the ICP-OES machine. Nine solutions of different NaI concentrations were prepared. These concentrations were 0, 0.1, 0.2, 0.5, 1, 2, 5, 10 and 20 ppm. These samples were analysed with the ICP-OES machine in order to get data to which a calibration curve could be fitted.[50] The samples containing the iodine captured in the filter test experiment were analysed using the ICP-OES machine when the iodine capture experiment has been performed. The samples were diluted by a factor 100 in order to fall into the range of 0-20 ppm which is appropriate for the ICP-OES machine that was used. In each run, some blank samples were introduced to the system to control memory effects. Before ICP-OES analysis, all samples were filtered in order to remove any big particles that would cause problems in the ICP-OES machine. This would essentially be charcoal particles.

4.5.2 Analysis of radioactive iodine

Each filter from the disassembled filter tubes were put into a sample vial which was placed in the HPGe detector. The activity of the radioactive methyl iodide captured by the filters was measured. Note that the livetime differs between the samples. The ones that had very low or no activity were in some cases measured for several hours.

4.6 Experimental setup

In this section the experimental setup for the active and passive sampling systems is described.

4.6.1 Active sampling

The experimental setup is shown in image 27. The power supply to which for the pump was connected to a voltmeter in order to monitor the voltage. This is important because the voltage range within which the pump can operate is 2-4 V, which is small compared to the power supply's capacity of 60 V. Also, the flow rate of the pump is directly proportional to the voltage. This part of the experimental setup is shown in figure **??**. The screw top vial containg $CH_3^{131}I$ is stored in a lead pot (to the far right in figure 27) in order to minimize

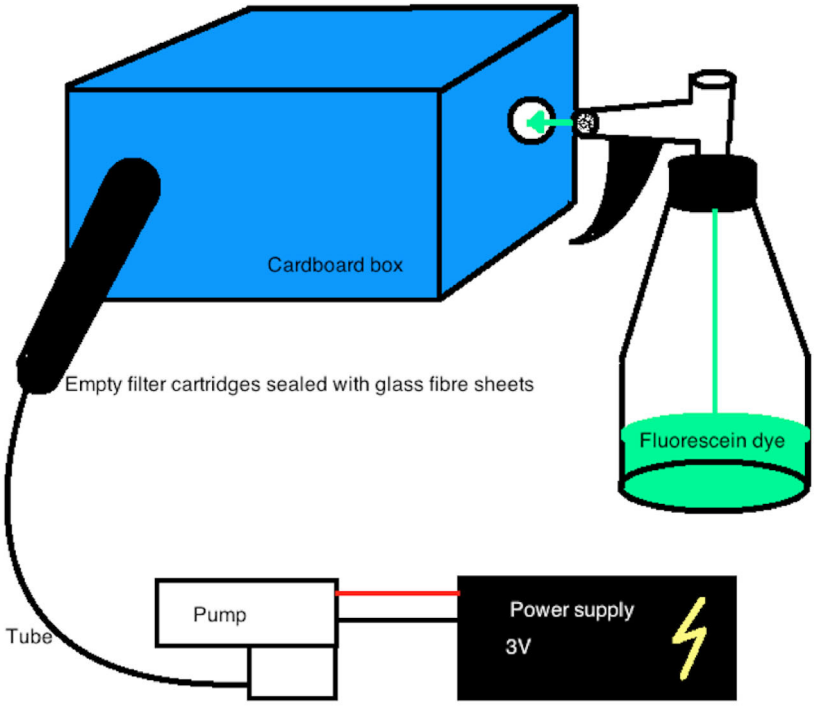

Figure 18: A schematic drawing of the setup for the dye experiment.

Figure 19: The spray bottle that was used for the dye experiment.

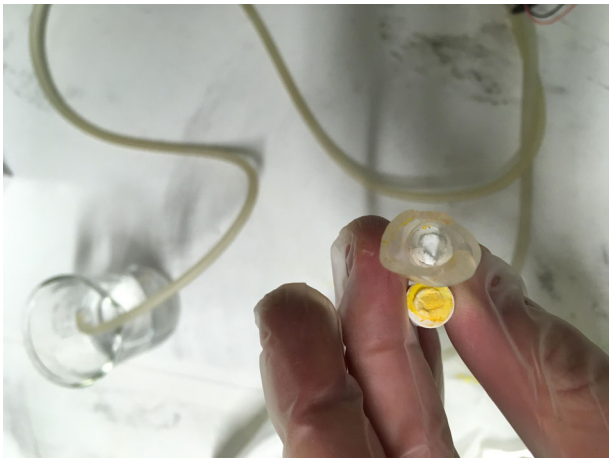

Figure 20: The first and second filter cartridges after the dye experiment.

Figure 21: Heating the shrink tube containing the filters.

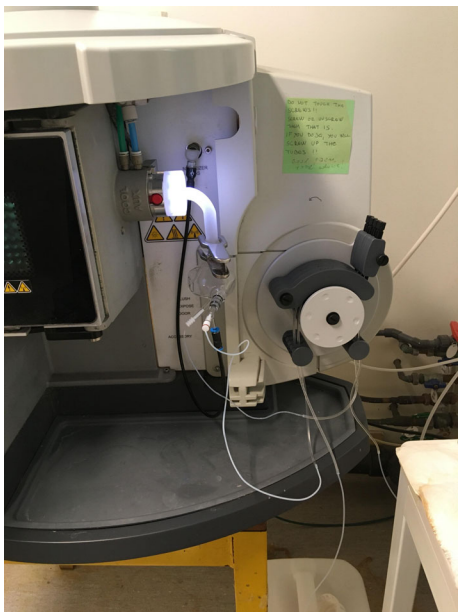

Figure 22: The ICP-OES machine in action.

Figure 23: The ICP-OES machine's automatic sampling system

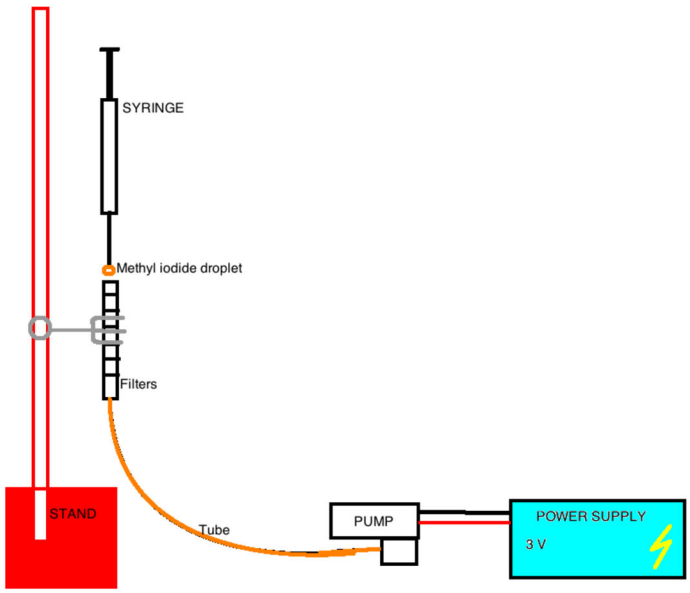

Figure 24: A schematic drawing of the setup for the methyl iodide sampling experiments.

unnecessary exposure to radiation. The count rate was measured with a Geiger detector close to the filter in order to get an indication that the methyl iodide had been successfully injected into the system, and not been spilled, escaped into the fumehood.

4.7 Experiments using radioactive iodine (^{131}I)

4.7.1 Unpacking the ^{131}I delivery, safety precaution

On the label in figure 25, it can be seen that the transport index was 0.4, which means that the radiation dose rate must not exceed 0.004 mSv/h at a 1 m distance from the package. The yellow "radioactive II" label indicates that the dose rate at the surface of the package is in the range 0.005-0.5 mSv/h.[51] When unpacking the delivery of ^{131}I, the dose rate was measured at different distances from the box, in order to verify the transport index. Once this was done, the can was unpacked. The ^{131}I was stored in a screw top vial in a thick lead-walled container, in the can. The activity of the delivered ^{131}I was 2.04 GBq.

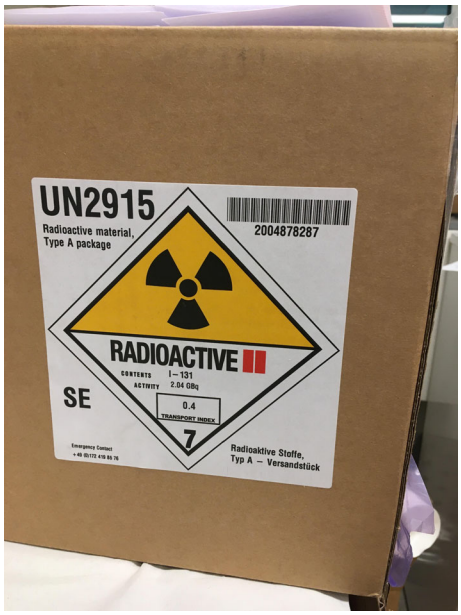

Figure 25: The box that the ^{131}I was delivered in.

Figure 26: The can that contains the ^{131}I

4.8 Synthesis of radioactive methyl iodide

Methyl iodide was synthesized according to reaction 9 using a distillation setup with some modifications for radiation protection. The ventilation system connected to the fumehood in which the synthesis was carried out has a series of filters. These prevent radioactive particles from being released into the general ventilation system. The vessel containg ^{131}I was kept in a lead pot during the whole synthesis, in order to minimize exposure to radiation. Figure 24 shows the distillation setup that was used for the synthesis.

A litter picker with gloves on it (shown in figure 28) was used for moving the vial containing the product, methyl iodide, of the reaction from the fumehood to an NaI-crystal scintillation detector in order for measurements of the activity. This is an example of a measure taken to minimize exposure to radiation, as opposed to holding the vial in one's hand.

4.9 Implementing the chemical sampling system into the drone

The weight of the pump is 45g and the weight of a filter system consisting of one filter cartridge filled with copper powder and five filter cartridges filled with DABCO-activated charcoal is 15g. The pump works in the voltage range 1-5 V, and it can either be powered by a separate power supply or the the power supply that is already included in the payload for powering the UAV. The weight of the Kromek GR1 γ-ray spectrometer is 59g, which makes it suitable to attach on the UAV. It is also USB-powered, so it can be connected to the built-in computer of the UAV. The Kromek GR1 is meant to be used as a "sniffing device", that can seek out

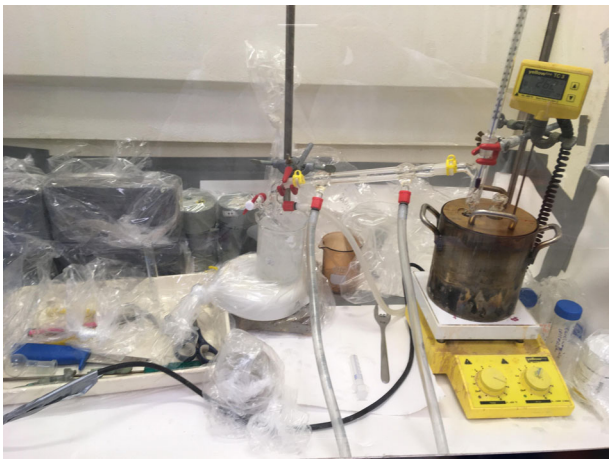

Figure 27: The experimental setup for producing $CH_3^{131}I$.

Figure 28: The litterpicker with gloves on which was used to transfer radioactive samples from the fumehood to the scintillation detector.

specific radionuclides to sample. When it senses the presence of the radionuclide sought to be sampled, the pump of the active sampling system

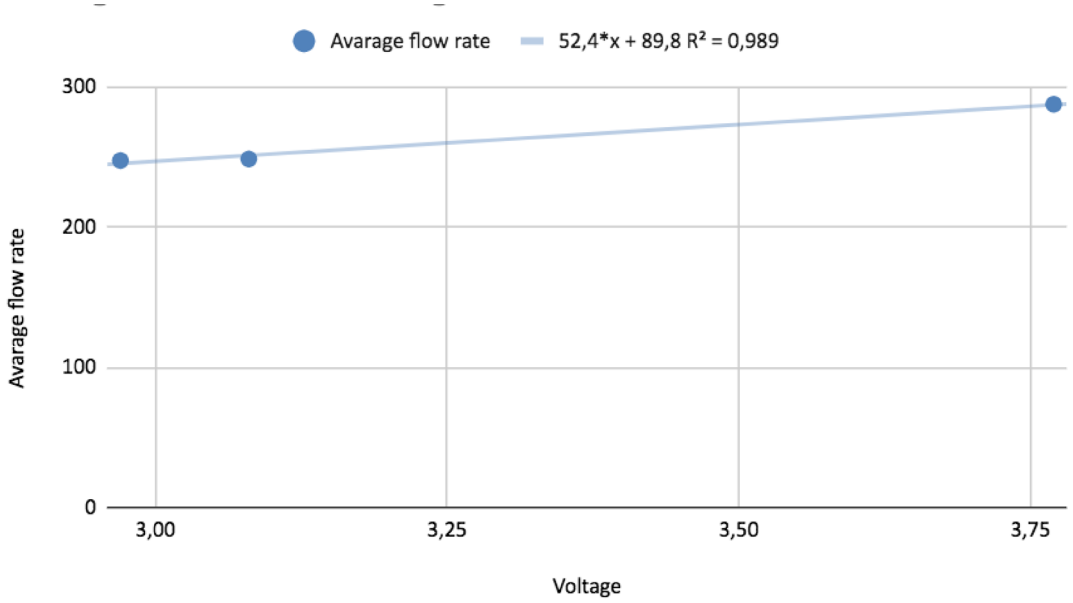

Figure 29: The straight line fitted to the data collected from measuring the flow rate of the pump at different voltages.

5 Results

5.0.1 Pump flow rate measurements

In figure 29, the measured flow rate of the pump is plotted against the input voltage. The linear equation which was fitted had a corresponding R^2-value of 0.989.

5.1 Results from ICP analysis

The calibration curve that was constructed from the ICP-OES measurements of the standard series of NaI solutions are shown in figure 30. These were used to calculate concentrations of iodine in the samples. In table 17, the percentage of the MPC (Maximum Prospective Concentration) is shown for all the filters that were tested in the non-radioactive CH_3I capture experiments. Complete calculations can be found in Appendix, in the section "ICP-OES Calculations". Filter 1 of run 1 was split up into four different samples, denoted I through IV in the table. This data is represented as bar charts in figures 36 through 40.

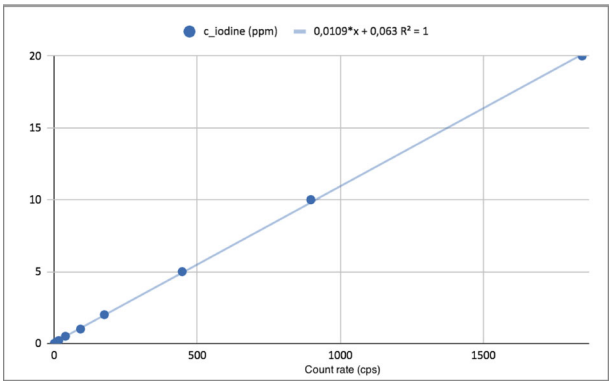

Figure 30: The ICP-OES calibration curve that was fitted to the data from analysing the concentration standard samples.

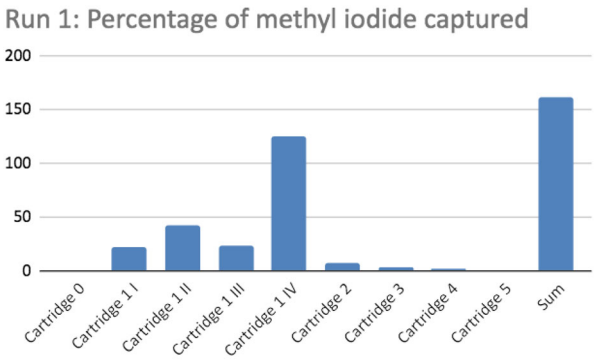

Figure 31: The percentage of the methyl iodide that was captured in each filter during the first run of the experiment, represented in a bar chart.

5.2 Results from HPGe analysis

For the passive filters that were tested, the count rate measured for each channel in the HPGe detector is shown in counts per second. Note the difference when the distance between sample and detector is increased. The results from run 1 of the active radioactive sampling of methyl iodide are shown in figures Radioactive runs 1 through 6 and the passive radioactive run are shown in figures 43 through 89, see appendix. In tables 4 thourhg 9, the total count rate (in cps) for each filter cartridge in radioactive runs 1 through 6 are displayed. In figures 36 through 41, the data is represented as bar charts. The results from the three radioactive active runs using passive filters are shown in table 3, and visualized in figures 42 and **??** as bar charts.

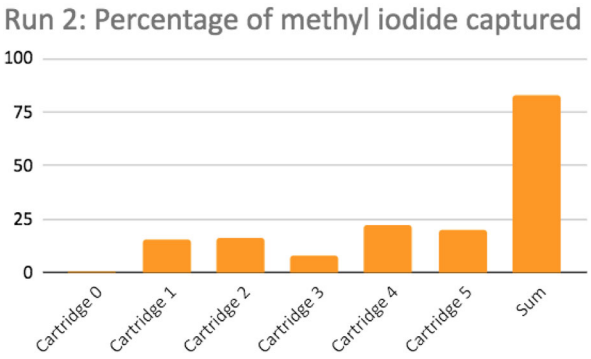

Figure 32: The percentage of the methyl iodide that was captured in each filter during the second run of the experiment, represented in a bar chart.

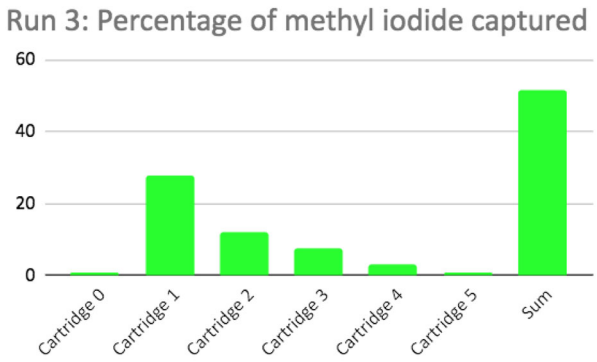

Figure 33: The percentage of the methyl iodide that was captured in each filter during the third run of the experiment, represented in a bar chart.

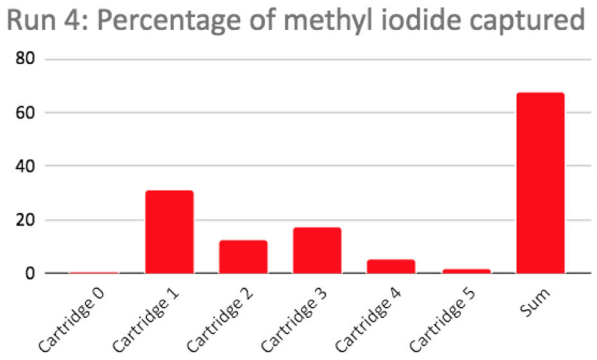

Figure 34: The percentage of the methyl iodide that was captured in each filter during the fourth run of the experiment, represented in a bar chart.

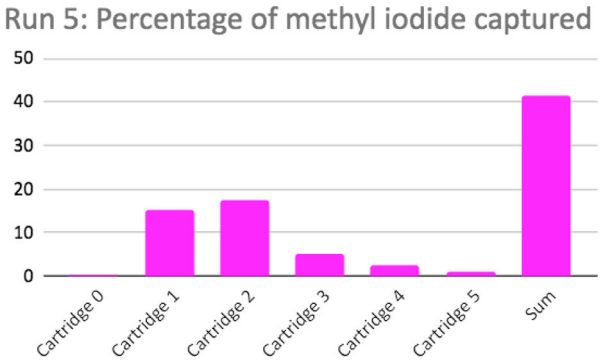

Figure 35: The percentage of the methyl iodide that was captured in each filter during the fifth run of the experiment, represented in a bar chart.

Table 3: The count rates measured for each passive filter.

Cartridge	Count rate (cps)
Filter 1	1804.2
Filter 2	1732.3
Filter 3	1841.1

Table 4: The count rates measured for each filter in radioactive run 1.

Cartridge	Count rate (cps)
Copper filter	0
Charcoal filter 1	1898.2
Charcoal filter 2	1917.2
Charcoal filter 3	206.6
Charcoal filter 4	0
Charcoal filter 5	0

Table 5: The count rates measured for each filter in radioactive run 2.

Cartridge	Count rate (cps)
Copper filter	0
Charcoal filter 1	122.0
Charcoal filter 2	0
Charcoal filter 3	0
Charcoal filter 4	0
Charcoal filter 5	0

Table 6: The count rates measured for each filter in radioactive run 3.

Cartridge	Count rate (cps)
Copper filter	0
Charcoal filter 1	3275.4
Charcoal filter 2	853.5
Charcoal filter 3	0
Charcoal filter 4	0
Charcoal filter 5	0

Table 7: The count rates measured for each filter in radioactive run 4.

Cartridge	Count rate (cps)
Copper filter	0
Charcoal filter 1	8398.3
Charcoal filter 2	306.2
Charcoal filter 3	0
Charcoal filter 4	0
Charcoal filter 5	0

Table 8: The count rates measured for each filter in radioactive run 5.

Cartridge	Count rate (cps)
Copper filter	3.3
Charcoal filter 1	5466.5
Charcoal filter 2	2285.9
Charcoal filter 3	15.4
Charcoal filter 4	0
Charcoal filter 5	0

Table 9: The count rates measured for each filter in radioactive run 6.

Cartridge	Count rate (cps)
Copper filter	3.3
Charcoal filter 1	4460.4
Charcoal filter 2	1014.9
Charcoal filter 3	75.1
Charcoal filter 4	0
Charcoal filter 5	0

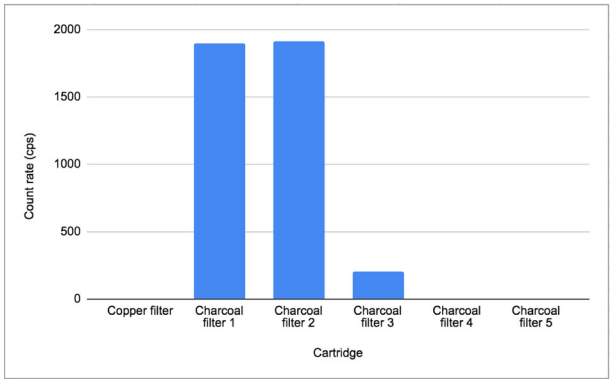

Figure 36: The count rates measured for each filter in radioactive run 1.

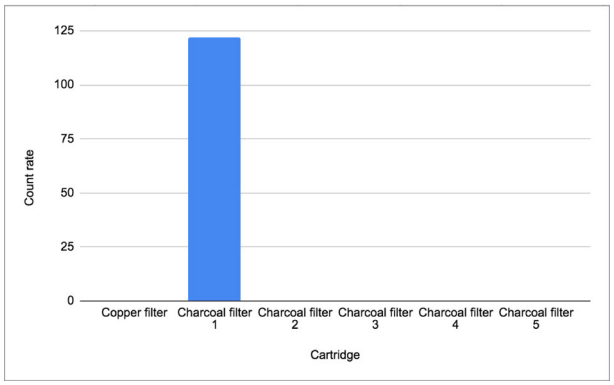

Figure 37: The count rates measured for each filter in radioactive run 2.

.

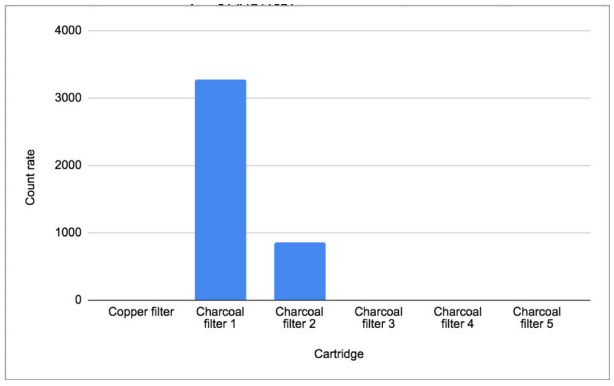

Figure 38: The count rates measured for each filter in radioactive run 3.

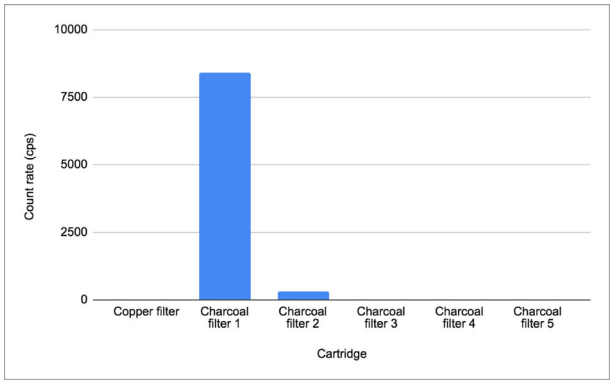

Figure 39: The count rates measured for each filter in radioactive run 4.

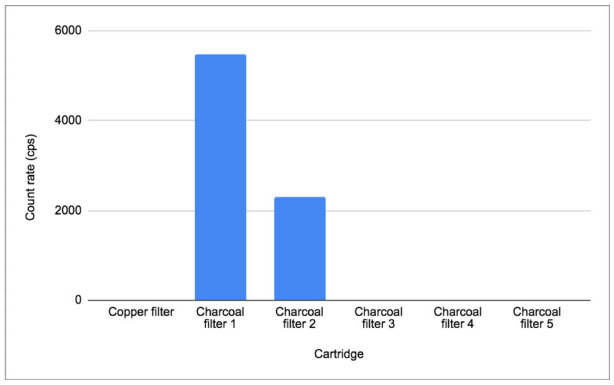

Figure 40: The count rates measured for each filter in radioactive run 5.

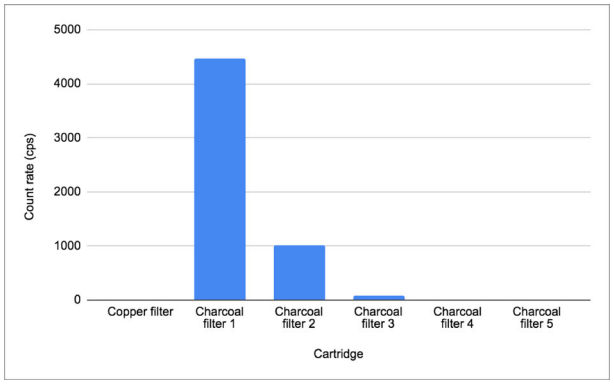

Figure 41: The count rates measured for each filter in radioactive run 6.

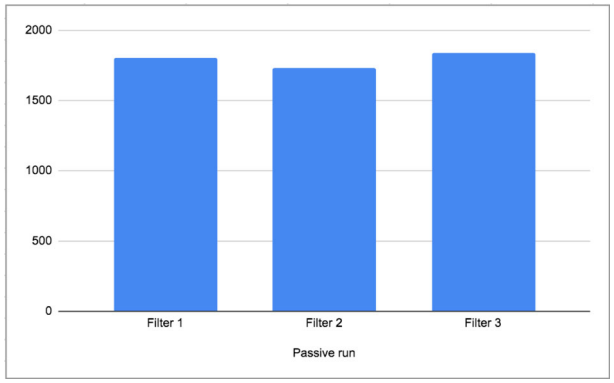

Figure 42: The count rates measured in cps for each passive filter.

6 Discussion

6.1 ICP-OES analysis

The results form the ICP analysis showed that the filters were capable of capturing significant amounts of iodine, but not as much as were expected. One of the filters was calculated to have captured 123 % of the methyl iodide that was introduced to the system, which is most probably the result of a mistake related to inaccurate use of the syringe, or erroneous documentation while diluting the samples before introducing them to the ICP-OES machine. Apart from this, the filter that had the best performance in the experiments captured 30% of what was expected given the methyl iodide capturing capability reported by Aneheim *et al.*[15].

6.2 HPGe analysis

With exception to radioactive runs 1 and 2, the results shown in figures 36 through 41 consistently show that little or no amounts of methyl iodide passed further than the first charcoal filter in the filter tube. The results for the passive sampling experiments show that they consistently capture significant quantities of methyl iodide. The assessment can be made that the filters are suitable for capturing methyl iodide.

6.3 Error and Error propagation analysis

Two different analysis techniques were used for the radioactive and non-radioactive samples: ICP-OES and γ-ray spectroscopy. These two give results in the form of spectra of different sorts: The ICP-OES analysis gives a spectrum of photons emitted by de-excitement of electrons, whereas the spectra obtained from γ-ray spectroscopy which displays photons emitted as a result of de-excitation of nuclei in excited states. With this comes the risk of getting different results, depending on which analysis technique was chosen. The results did vary significantly between ICP-OES analysis and the γ-ray spectroscopy. However, the purpose of the sampling system is to sample radionuclides, and thus γ-ray spectroscopy is the preferred method as it differentiates between the different isotopes of the same element. For example, this is imperative if one were to sample ^{134}Cs, ^{135}Cs and ^{137}Cs and use the ratios between these for investigating the source of the radionuclides released as a result of a NPP accident. During the active sampling experiments, it can affect the result if the pump is not operating at a steady flow rate. During operation, the input voltage was monitored using a voltmeter so it could be ensured that there were no significant deviations in the flow rate. By placing the blowing end of the tube in a beaker filled with water and monitoring the bubbling, it was ensured that there were no leakages of gas in the system. Thus the pump is not considered a significant source of error. The methyl iodide was introduced to the system by means of a syringe and the droplet was placed on top of a glass fibre sheet. Likely because of air being sucked into the syringe while sucking in the methyl iodide, the volume injected was too small in radioactive runs 1 and 2, as the total amount of methyl iodide captured by the filters is much smaller than that of radioactive runs 3 through 6. Another source of error is the fact that the methyl iodide vapor had the potential of escaping into the fumehood instead of being sucked through the glass fibre sheet. This way some of the methyl iodide capture efficiency could go lost.

6.4 Evaluation of the components of the system

The assessment for the DABCO-loaded charcoal is that they are suitable for capturing methyl iodide. Based on the flow rate measurements, the pump was assessed to fulfill the maximum flow rate specification of 380 l/min. The pump was not considered a source of error in the active sampling experiments. The accuracy of the Kromek GR1 γ-radiation spectrometer was not investigated. Its purpose is to guide the UAV towards the radionuclides of interest to be sampled, rather than to perform accurate measurements of the activity. If it can accurately distinguish different isotopes from each other, it will fulfill this purpose. When flying the UAV, it is important to avoid extreme temperatures because the Kromek GR1 γ-ray spectrometer as the temperature range in which it can operate is 0-40°C. This could potentially cause problems if the UAV flies close to a nuclear reactor which recently exploded and the temperature is high. A filter tube containing five charcoal filters and one copper filter weighed 15 g, the weight of the pump was 45 g and the weight of the Kromek GR1 is 58.9g. The power consumption of the pump and the GR1 is 480 mW and 250 mW respectively. These components are light and have low power consumption, so there should be no problem for the UAV to carry and power this payload.

6.5 Future work

More research is yet to be conducted in sampling systems for radionuclides. Making filters for sampling other radionuclides than ^{131}I, such as ^{137}Cs, could be investigated in the future. The results of this project can be regarded as successful; the filters that were made were suitable for the purpose of sampling methyl iodide

and the components that were chosen for the sampling system were light and have low power consumption. However a UAV flight employing the sampling system has yet to be conducted to see if the sampling system has any unforeseen issues that need to be addressed. The practical utilisation of the sampling system and the UAV has not been investigated in this project. One of the main tasks that is desired to be carried out by the sampling system and the UAV is to locate hotspots of radioactivity. For this purpose, the GR1 was chosen to be fitted on the UAV. The accuracy of the Kromek GR1 has yet to be investigated when it is operated on a UAV. In order to protect the Kromek Gr1 from extreme temperatures, constructing a thermal shielding box for it could be looked into. To summarise, in future work, it needs to be investigated how well the components can be integrated in the UAV. Another idea for future work is to develop an autonomous piloting system for the UAV which guides it towards higher radioactivity and, at the same time, avoids walls and other obstacles that might come in its way. This poses the question of whether having a human pilot operate the UAV or using an autonomous piloting system is more suitable. The answer is likely to be a UAV that can be piloted both ways, depending on the situation. For example, while flying through a narrow space, an autonomous piloting system might be more suitable. Thus, an investigation on how the UAV handles different flying situations may be conducted in the future.

7 Conclusion

Filters for capturing I_2 and CH_3I, containing copper granules and DABCO-loaded charcoal have been manufactured with cost-efficient materials: Cylindric plastic beads, fabric and glass fibre sheets. Their capability of capturing methyl iodide has been tested both with and without a pump sucking in air through them. In order to obtain results from the experiments, the content of the filters were analysed in an ICP-OES machine and a HPGe detector. These two different analysis techniques yielded different results, but both consistently showed that the filters were suitable for capturing methyl iodide. In this way different isotopes of iodine could be sampled, both passively and actively. A sampling system to be attached on a UAV has been formulated. The components have been selected with respect to the payload capacity and size of the UAV. The parts of the system weigh a total of 119 g, which clears the UAV's payload limitation of 2 kg by a large margin. With respect to weight, the sampling system is well adapted to be implemented on the drone. However, a test flight with the sampling system has yet to be conducted. The system's viability in harsh weather conditions has yet to be investigated. This project is intended as a proof of concept of a system for sampling radionuclides attached on a UAV. For future studies on this area, filters designed to sample other radionuclides than ^{131}I, such as ^{137}Cs, can be developed.

8 Ackonowledgements

I would like to express my thankfulness to my supervisors who made this possible: Professor Teodora Retegan Vollmer, Associate Professor Mark Foreman and Santiago Arellano. I would like to thank you for all your time and dedication! It has been a great learning experience for me. I would also like to thank my examiner Professor Christian Ekberg.

Bibliography

[1] Norman. *Chernobyl: Errors and design flaws*. 1986.

[2] Mould. *Chernobyl record: the definitive history of the Chernobyl catastrophe*. CRC Press, 2000.

[3] Rudling et al. "Nuclear fuel behaviour under ria conditions". In: *Advanced Nuclear Technology International, Mölnlycke* (2016).

[4] Pöllänen, Valkama, and Toivonen. "Transport of radioactive particles from the Chernobyl accident". In: *Atmospheric Environment* 31.21 (1997), pp. 3575–3590.

[5] Atwood. "Chernobyl-what happened?" In: *Journal of Chemical Education* 65.12 (1988), p. 1037.

[6] Su'ud and Anshari. "Preliminary analysis of loss-of-coolant accident in Fukushima nuclear accident". In: *AIP Conference Proceedings*. Vol. 1448. 1. American Institute of Physics. 2012, pp. 315–327.

[7] Aoyama et al. "134 Cs and 137 Cs in the North Pacific Ocean derived from the March 2011 TEPCO Fukushima Dai-ichi nuclear power plant accident, Japan. Part two: estimation of 134 Cs and 137 Cs inventories in the North Pacific Ocean". In: *Journal of Oceanography* 72.1 (2016), pp. 67–76.

[8] Agoston Restas et al. "Drone applications for supporting disaster management". In: *World Journal of Engineering and Technology* 3.03 (2015), p. 316.

[9] Cai et al. "Designing a radiation sensing UAV system". In: *2016 IEEE Systems and Information Engineering Design Symposium (SIEDS)*. IEEE. 2016, pp. 165–169.

[10] Galle et al. "A multi-purpose, multi-rotor drone system for long range and high-altitude volcanic gas plume measurements". In: *Atmospheric Measurement Techniques Discussions* (2020), pp. 1–33.

[11] Magomedbekov and Obruchikov. "A method for properties evaluation of activated charcoal sorbents in iodine capture under dynamic conditions". In: *Nuclear Engineering and Technology* 51.2 (2019), pp. 641–645.

[12] Jie et al. "Reversible iodine capture by nonporous pillar [6] arene crystals". In: *Journal of the American Chemical Society* 139.43 (2017), pp. 15320–15323.

[13] Liao et al. "Highly efficient and reversible iodine capture in hexaphenylbenzene-based conjugated microporous polymers". In: *Macromolecules* 49.17 (2016), pp. 6322–6333.

[14] Matsui, Noguchi, and Yoshida. "Production of elemental iodine from radioactive methyl iodide under sunlight". In: *Journal of Nuclear Science and Technology* 16.7 (1979), pp. 527–530.

[15] Aneheim, Bernin, and Foreman. "Affinity of charcoals for different forms of radioactive organic iodine". In: *Nuclear Engineering and Design* 328 (2018), pp. 228–240.

[16] Beahm et al. "Organic iodide formation during severe accidents in light water nuclear reactors". In: *Nuclear technology* 78.1 (1987), pp. 34–42.

[17] Youn et al. "Potential impact of iodinated replacement compounds CF 3 I and CH 3 I on atmospheric ozone: a three-dimensional modeling study". In: *Atmospheric Chemistry and Physics* 10.20 (2010), pp. 10129–10144.

[18] Zheng et al. "135Cs/137Cs isotopic ratio as a new tracer of radiocesium released from the Fukushima nuclear accident". In: *Environmental science & technology* 48.10 (2014), pp. 5433–5438.

[19] Pudykiewicz. "Numerical simulation of the transport of radioactive cloud from the Chernobyl nuclear accident". In: *Tellus B: Chemical and Physical Meteorology* 40.4 (1988), pp. 241–259.

[20] Misaelides et al. "Distribution of fission products in dust samples from the region of Thessaloniki, Greece, after the Chernobyl nuclear accident". In: *Environmental Pollution* 47.1 (1987), pp. 1–8.

[21] Williams. "Radiation carcinogenesis: lessons from Chernobyl". In: *Oncogene* 27.2 (2008), S9–S18.

[22] Chino et al. "Preliminary estimation of release amounts of 131I and 137Cs accidentally discharged from the Fukushima Daiichi nuclear power plant into the atmosphere". In: *Journal of nuclear science and technology* 48.7 (2011), pp. 1129–1134.

[23] Yılmaz and Gürol. "Efficient removal of iodine-131 from radioactive waste by nanomaterials". In: *Instrumentation Science & Technology* 49.1 (2021), pp. 45–54.

[24] Braverman et al. "Managing terrorism or accidental nuclear errors, preparing for iodine-131 emergencies: a comprehensive review". In: *International journal of environmental research and public health* 11.4 (2014), pp. 4158–4200.

[25] Tokonami et al. "Thyroid doses for evacuees from the Fukushima nuclear accident". In: *Scientific Reports* 2.1 (2012), pp. 1–4.

[26] Holm. “Thyroid cancer after exposure to radioactive 131I”. In: *Acta Oncologica* 45.8 (2006), pp. 1037–1040.

[27] Fard-Esfahani et al. “Adverse effects of radioactive iodine-131 treatment for differentiated thyroid carcinoma”. In: *Nuclear medicine communications* 35.8 (2014), pp. 808–817.

[28] V Saenko et al. “The Chernobyl accident and its consequences”. In: *Clinical Oncology* 23.4 (2011), pp. 234–243.

[29] Allard and Skarnemark. *Radiation Protection Booklet, Department of Nuclear Chemistry, Chalmers University of Technology*. 2019.

[30] Didi, Dadouch, and El Bekkouri. “Feasibility study for production of iodine-131 using dioxide of tellurium-130”. In: *Int. J. Pharm. Pharmaceut. Sci* 8.327 (2016), e331.

[31] Tietze, Foreman, and Ekberg. “Synthesis of I-131 labelled iodine species relevant during severe nuclear accidents in light water reactors”. In: *Radiochimca Acta* 101.10 (2013), pp. 675–680.

[32] Vance et al. “Immobilization of iodine via copper iodide”. In: *Journal of Nuclear Materials* 505 (2018), pp. 143–148.

[33] Megaw and May. “The behaviour of iodine released in reactor containers”. In: *Journal of Nuclear Energy. Parts A/B. Reactor Science and Technology* 16.9 (1962), pp. 427–436.

[34] Foreman. “Reactor accident chemistry an update”. In: *Cogent Chemistry* 4.1 (2018), p. 1450944.

[35] Kitani, Tadami Noro, and Takaaki Kohara. “Removal of methyl iodide by impregnated charcoals from flowing air under humid condition”. In: *Journal of Nuclear Science and Technology* 9.4 (1972), pp. 197–202.

[36] Kromek Group plc. *GR1-A® and GR1® the World’s Smallest and Highest Resolution Room Temperature Gamma-Ray Spectrometers*. 2018.

[37] Kazemeini et al. “Gamma ray measurements using unmanned aerial systems”. In: *Use of Gamma Radiation Techniques in Peaceful Applications* (2019), p. 85.

[38] Pearson. “An improved calcium flame test”. In: *Journal of Chemical Education* 62.7 (1985), p. 622.

[39] Barnard and Chayen. *Modern methods of chemical analysis*. McGraw-Hill, 1965.

[40] *Agilent Technologies, ICP-OES FAQ’s including The ICP-OES Principle, ICP-OES Instrument and ICP-OES Analysis*. `https://www.agilent.com/en/support/icp-oes/icp-oes-instruments/icp-oes-faq`. Accessed: 2021-04-19.

[41] Ruzik. “Speciation of challenging elements in food by atomic spectrometry”. In: *Talanta* 93 (2012), pp. 18–31.

[42] Wheal and Palmer. “Chloride analysis of botanical samples by ICP-OES”. In: *Journal of Analytical Atomic Spectrometry* 25.12 (2010), pp. 1946–1952.

[43] Bechlin et al. “Contributions on the use of bismuth as internal standard for lead determinations using ICP-based techniques”. In: *Journal of the Brazilian Chemical Society* 26.9 (2015), pp. 1879–1886.

[44] Gold Book. “Compendium of chemical terminology”. In: *International Union of Pure and Applied Chemistry* 528 (2014).

[45] Wallbrink, Walling, and He. “Radionuclide measurement using HPGe gamma spectrometry”. In: *Handbook for the assessment of soil erosion and sedimentation using environmental radionuclides*. Springer, 2002, pp. 67–96.

[46] Browne, Firestone, and Shirley. “Table of radioactive isotopes”. In: (1986).

[47] Choppin, Liljenzin, and Rydberg. *Radiochemistry and nuclear chemistry*. Butterworth-Heinemann, 2002, pp. 250–253.

[48] Hardy et al. “Precise efficiency calibration of an HPGe detector: source measurements and Monte Carlo calculations with sub-percent precision”. In: *Applied Radiation and Isotopes* 56.1-2 (2002), pp. 65–69.

[49] Maier. “PREPARATION OF C-TARGETS BY CRACKING OF CH3–J”. In: *Preparation of Nuclear Targets for Particle Accelerators* (2013), p. 151.

[50] Inc. PerkinElmer. *Simplify your ICP-OES Sample Preparation*. Youtube. 2016. URL: `https://www.youtube.com/watch?v=yvWIy-fDyuA`.

[51] Saha. “Transportation of Radioactive Material”. In: *Radiation Safety in Nuclear Medicine*. Springer, 2019, pp. 149–156.

9 Appendix

Extensive experimental results and calculations that would take up a lot of space in the report are shown in this section.

9.1 Extensive results from HPGe detector measurements

In figures 43 through 89, the emitted γ-ray spectrum from each filter cartridge used for the $CH_3^{131}I$-sampling experiments are shown. These spectra show the number of counts per second measured for each energy channel on the HPGe machine. The distinct peak which appears at approximately channel 1390 corresponds to 364,483 eV, the peak that makes up 81,2 % of the γ-radiation energy released during decay. The count rate of ^{131}I was determined by summing up the count rate measured for the energy channels that were considered to contribute to the aforementioned energy peak.

9.2 Missing data points

One of the copper filters broke open during the disassembly of the filter tube in run 4 of the $CH_3^{131}I$- capture experiments. This caused copper powder to spread out but it was contained in the fumehood and no person or object outside the fumehood was contaminated. The copper powder in the fumehood was collected using duct tape, bagged and put with the rest of the waste from the fumehood.

9.3 ICP-OES calculations

Tables 10 through 16 show the calculations that were performed to yield table 16, whose values are presented as bar charts in the results section, see figures 36 through 40. The samples that were prepared for the ICP-OES analysis were to be filtered and diluted. Because of mistakes being made, the samples had to be diluted twice. The weight of the filtered solution was not recorded and because of this, addition calculations had to be made. The vials and their caps were all assumed to have the same weight in order to simplify the calculations. Instead the weights of the vials filled with samples, diluted once and twice respectively, were weighed. To calculated the weight of filtered solution, $m_{filtered}$, the weight of an empty vial, m_{empty} was subtracted from the weight of the filled vial, m_{filled}, as seen in equtaion 10. The fraction of the solution that was filtered, denoted F in equation 11, was calculated by dividing the weight of filtered solution, m_F, by the weight of the solution when it had been diluted twice, m_D. The concentration of iodine in the samples that were diluted once were calculated by inserting the measured count rate into the equation for the calibration curve. Equation 12 corresponds to the calibration curve, where c is the concentration in ppm and r is the count rate. The curve was constructed from the data points collected for the samples of the standard NaI-concentration series.

$$m_{filtered} = m_{filled} - m_{empty} \tag{10}$$

$$F = \frac{m_F}{m_D} \tag{11}$$

$$c = 0,0109 * r + 0,063 \tag{12}$$

9.4 Data from experiments

Table 10: Weighth of caps, empty vials with and without caps respectively.

Filter Cartridge	Weights of empty (g) vials with cap	Emptied. no cap (g)	Cap (g)
Run 1			
0	6.71501	5.44622	1.26879
1 I	6.71501	5.44622	1.26879
1 II	6.71501	5.44622	1.26879
1 III	6.71501	5.44622	1.26879
1 IV	6.71501	5.44622	1.26879
2	6.71501	5.44622	1.26879
3	6.71501	5.44622	1.26879
4	6.71501	5.44622	1.26879
5	6.71501	5.44622	1.26879
Run 2			
0	6.71501	5.44622	1.26879
1	6.71501	5.44622	1.26879
2	6.71501	5.44622	1.26879
3	6.71501	5.44622	1.26879
4	6.71501	5.44622	1.26879
5	6.71501	5.44622	1.26879
Run 3			
0	6.71501	5.44622	1.26879
1	6.71501	5.44622	1.26879
2	6.71501	5.44622	1.26879
3	6.71501	5.44622	1.26879
4	6.71501	5.44622	1.26879
5	6.71501	5.44622	1.26879
Run 4			
0	6.71501	5.44622	1.26879
1	6.71501	5.44622	1.26879
2	6.71501	5.44622	1.26879
3	6.71501	5.44622	1.26879
4	6.71501	5.44622	1.26879
5	6.71501	5.44622	1.26879
Run 5			
0	6.71501	5.44622	1.26879
1	6.71501	5.44622	1.26879
2	6.71501	5.44622	1.26879
3	6.71501	5.44622	1.26879
4	6.71501	5.44622	1.26879
5	6.71501	5.44622	1.26879

.

Table 11: Weights of vials after adding ICP-OES matrix solution once and twice respectively.

Filter Cartridge	Diluted once (g)	Diluted twice (g)	Weight of liquid filtered into ICP tube (g)
Run 1			
0	11.4407	17.4674	4.72569
1 I	8.7132	18.7034	1.99819
1 II	8.2281	18.1892	1.51309
1 III	9.5699	19.5422	2.85489
1 IV	8.1025	18.0636	1.38749
2	11.4033	18.4223	4.68829
3	10.9674	17.9737	4.25239
4	10.17	17.1844	3.45499
5	10.8262	17.8295	4.11119
Run 2			
0	12.1361	18.1564	5.42109
1	11.6302	18.6145	4.91519
2	11.4263	18.4088	4.71129
3	12.0402	19.0272	5.32519
4	10.4109	17.38	3.69589
5	11.5086	18.5044	4.79359
Run 3			
0	12.1421	18.1623	5.42709
1	11.7802	18.7161	5.06519
2	11.8464	18.8461	5.13139
3	12.0176	19.0062	5.30259
4	11.6602	18.671	4.94519
5	12.3349	19.3482	5.61989
Run 4			
0	14.9007	20.9211	8.18569
1	11.4434	18.398	4.72839
2	12.6749	19.6784	5.95989
3	11.5673	18.5672	4.85229
4	11.3747	18.3695	4.65969
5	11.6656	18.6611	4.95059
Run 5			
0	14.209	20.2295	7.49399
1	12.4853	19.4658	5.77029
2	12.7453	19.7488	6.03029
3	12.9791	19.9849	6.26409
4	11.9338	18.9342	5.21879
5	11.7028	18.6941	4.98779

Table 12: Calculations for ICP-OES results. continued.

Filter Cartridge	Weight of NH_3 solution added after filtering sample (g)	Fraction of solution filtered	n_iodine_max (
Run 1			
0	6.0267	0.472569	0.0003
1 I	9.9902	0.199819	0.0003
1 II	9.9611	0.151309	0.0003
1 III	9.9723	0.285489	0.0003
1 IV	9.9611	0.138749	0.0003
2	7.019	0.468829	0.0003
3	7.0063	0.425239	0.0003
4	7.0144	0.345499	0.0003
5	7.0033	0.411119	0.0003
Run 2			
0	6.0203	0.542109	0.0003
1	6.9843	0.491519	0.0003
2	6.9825	0.471129	0.0003
3	6.987	0.532519	0.0003
4	6.9691	0.369589	0.0003
5	6.9958	0.479359	0.0003
Run 3			
0	6.0202	0.542709	0.0003
1	6.9359	0.506519	0.0003
2	6.9997	0.513139	0.0003
3	6.9886	0.530259	0.0003
4	7.0108	0.494519	0.0003
5	7.0133	0.561989	0.0003
Run 4			
0	6.0204	0.818569	0.0003
1	6.9546	0.472839	0.0003
2	7.0035	0.595989	0.0003
3	6.9999	0.485229	0.0003
4	6.9948	0.465969	0.0003
5	6.9955	0.495059	0.0003
Run 5			
0	6.0205	0.749399	0.0003
1	6.9805	0.577029	0.0003
2	7.0035	0.603029	0.0003
3	7.0058	0.626409	0.0003
4	7.0004	0.521879	0.0003
5	6.9913	0.498779	0.0003

Table 13: Calculations for ICP-OES results. continued.

Filter Cartridge	Weight of ammonia solution added after filtering sample (g)	Fraction of solution filtered
Run 1		
0	6.0267	0.472569
1 I	9.9902	0.199819
1 II	9.9611	0.151309
1 III	9.9723	0.285489
1 IV	9.9611	0.138749
2	7.019	0.468829
3	7.0063	0.425239
4	7.0144	0.345499
5	7.0033	0.411119
Run 2		
0	6.0203	0.542109
1	6.9843	0.491519
2	6.9825	0.471129
3	6.987	0.532519
4	6.9691	0.369589
5	6.9958	0.479359
Run 3		
0	6.0202	0.542709
1	6.9359	0.506519
2	6.9997	0.513139
3	6.9886	0.530259
4	7.0108	0.494519
5	7.0133	0.561989
Run 4		
0	6.0204	0.818569
1	6.9546	0.472839
2	7.0035	0.595989
3	6.9999	0.485229
4	6.9948	0.465969
5	6.9955	0.495059
Run 5		
0	6.0205	0.749399
1	6.9805	0.577029
2	7.0035	0.603029
3	7.0058	0.626409
4	7.0004	0.521879
5	6.9913	0.498779

Table 14: Calculations for ICP-OES results. continued.

Filter Cartridge	Weight of ammonia solution added after filtering sample (g)	Fraction of solution filtered
Run 1		
0	6.0267	0.472569
1 I	9.9902	0.199819
1 II	9.9611	0.151309
1 III	9.9723	0.285489
1 IV	9.9611	0.138749
2	7.019	0.468829
3	7.0063	0.425239
4	7.0144	0.345499
5	7.0033	0.411119
Run 2		
0	6.0203	0.542109
1	6.9843	0.491519
2	6.9825	0.471129
3	6.987	0.532519
4	6.9691	0.369589
5	6.9958	0.479359
Run 3		
0	6.0202	0.542709
1	6.9359	0.506519
2	6.9997	0.513139
3	6.9886	0.530259
4	7.0108	0.494519
5	7.0133	0.561989
Run 4		
0	6.0204	0.818569
1	6.9546	0.472839
2	7.0035	0.595989
3	6.9999	0.485229
4	6.9948	0.465969
5	6.9955	0.495059
Run 5		
0	6.0205	0.749399
1	6.9805	0.577029
2	7.0035	0.603029
3	7.0058	0.626409
4	7.0004	0.521879
5	6.9913	0.498779

Table 15: Calculations for ICP-OES results. continued.

Filter Cartridge	Cps iodine measured	n_iodine (ppm) actually measured
Run 1		
0	0.2421091	0.065638989
1 I	23.92068627	0.32373548
1 II	26.9727674	0.357003165
1 III	51.92325929	0.628963526
1 IV	76.76773043	0.899768262
2	50.92407481	0.618072415
3	17.1605081	0.250049538
4	0.61722011	0.069727699
5	0.117758792	0.064283571
Run 2		
0	0.41067306	0.067476336
1	115.474472	1.321671745
2	116.3150285	1.33083381
3	67.51611522	0.798925656
4	103.7588939	1.193971944
5	148.6943721	1.683768656
Run 3		
0	0.497365725	0.068421286
1	223.5798787	2.500020678
2	95.42318949	1.103112765
3	62.76935446	0.747185964
4	19.30792887	0.273456425
5	0.688397464	0.070503532
Run 4		
0	0.024434671	0.063266338
1	224.2125372	2.506916656
2	125.8947936	1.435253251
3	128.3874877	1.462423616
4	31.94685099	0.411220676
5	4.565096059	0.112759547
Run 5		
0	0.273084988	0.065976626
1	148.7960371	1.684876805
2	182.788698	2.055396808
3	52.4023854	0.634186001
4	17.04795913	0.248822754
5	3.087224827	0.096650751

Table 16: Calculations for ICP-OES results. continued.

Filter cartridge	ppm Iodine in the sample before being diluted for the first time(mol)	% captured of MPC
Run 1		
0	0.1388982121	0.74220808
1 I	1.620143632	22.82794633
1 II	2.359431128	42.01978482
1 III	2.203109494	23.24702986
1 IV	6.484863038	124.5667391
2	1.318332303	7.731362664
3	0.5880211794	3.656259275
4	0.2018173691	1.436224619
5	0.1563624421	0.9927586483
	Sum:	161.6303742
Run 2		
0	0.1244700537	0.6169447776
1	2.68895352	15.28834858
2	2.824775827	16.46602172
3	1.500276339	8.146305715
4	3.230539718	21.89302353
5	3.512542073	20.288093
	Sum:	82.69873732
Run 3		
0	0.1260736166	0.6245239761
1	4.935689832	27.46389026
2	2.1497348	11.93545367
3	1.409096241	7.670713871
4	0.5529745565	3.139763619
5	0.1254535807	0.6623042127
	Sum:	51.49664961
Run 4		
0	0.07728894926	0.3150111416
1	5.301839856	30.76497479
2	2.408187484	12.30155127
3	3.013883375	17.28890716
4	0.8825065096	5.183742373
5	0.2277699164	1.290786539
	Sum:	67.14497327
Run 5		
0	0.08803938406	0.3728660059
1	2.919917032	15.15302038
2	3.408454333	17.30132021
3	1.012415213	5.036829377
4	0.476782462	2.621694672
5	0.193774699	1.092954247
	Sum:	41.5786849

Table 17: The final result of the calculations. that is the percentage of the MPC in the filters.

Filter cartridge	% captured of MPC
Run 1	
0	0.74220808
1 I	22.82794633
1 II	42.01978482
1 III	23.24702986
1 IV	124.5667391
2	7.731362664
3	3.656259275
4	1.436224619
5	0.992758648
Sum of run 1:	161.6303742
Run 2	
0	0.616944778
1	15.28834858
2	16.46602172
3	8.146305715
4	21.89302353
5	20.288093
Sum of run 2:	82.69873732
Run 3	
0	0.624523976
1	27.46389026
2	11.93545367
3	7.670713871
4	3.139763619
5	0.662304213
Sum of run 3:	51.49664961
Run 4	
0	0.315011142
1	30.76497479
2	12.30155127
3	17.28890716
4	5.183742373
5	1.290786539
Sum of run 4:	67.14497327
Run 5	
0	0.372866006
1	15.15302038
2	17.30132021
3	5.036829377
4	2.621694672
5	1.092954247
Sum of run 5:	41.5786849

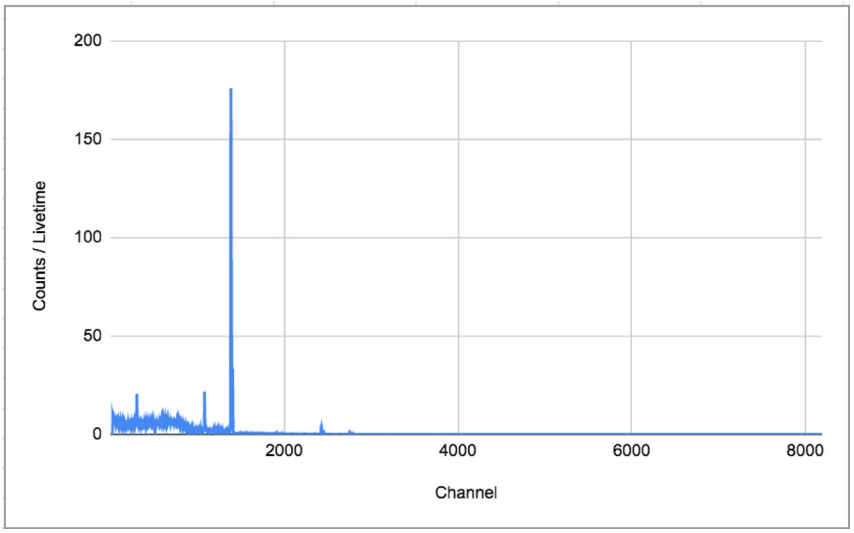

Figure 43: The emitted γ-ray spectrum from filter cartridge 1 in the passive run.

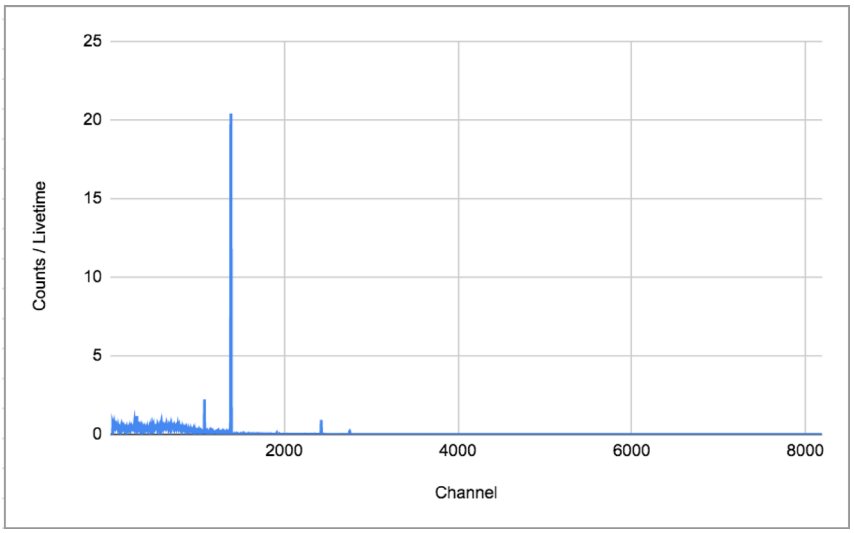

Figure 44: The emitted γ-ray spectrum from charcoal filter cartridge 1 in the passive run when the distance from the detector crystal was increased.

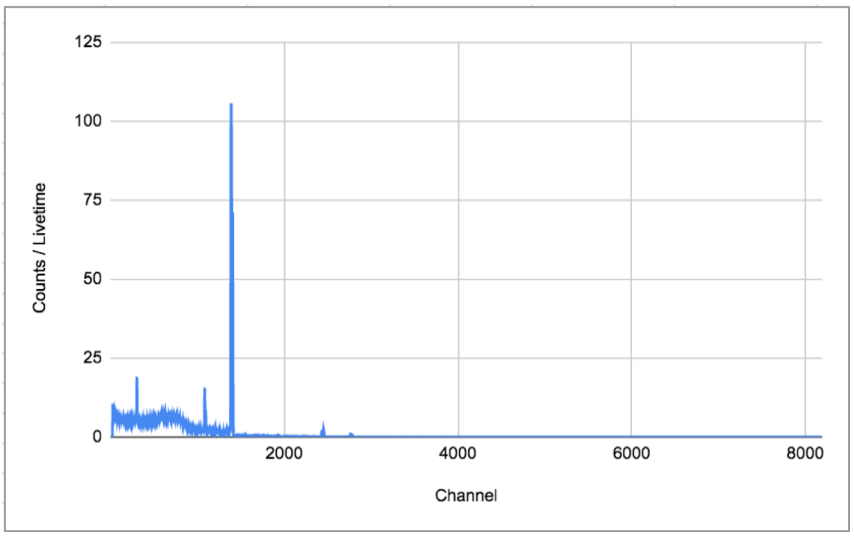

Figure 45: The emitted γ-ray spectrum from charcoal filter cartridge 2 in the passive run.

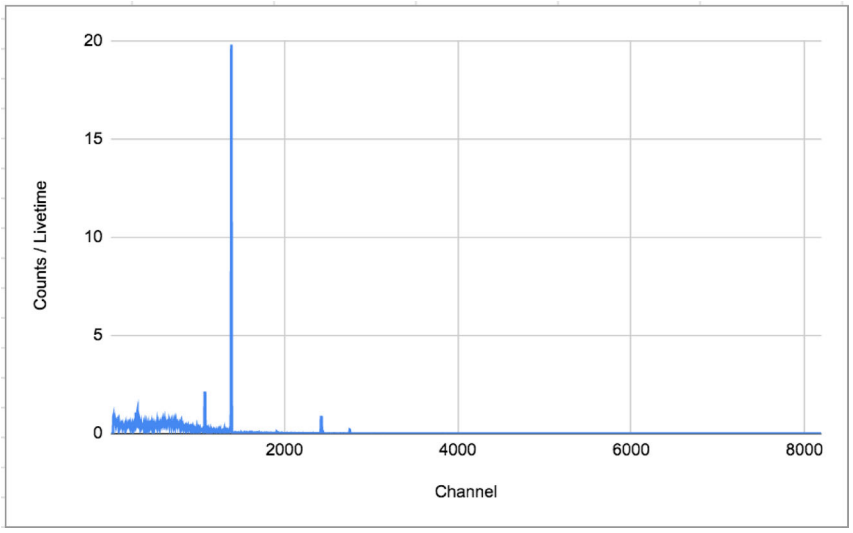

Figure 46: The emitted γ-ray spectrum from charcoal filter cartridge 2 in the passive run when the distance from the detector crystal was increased.

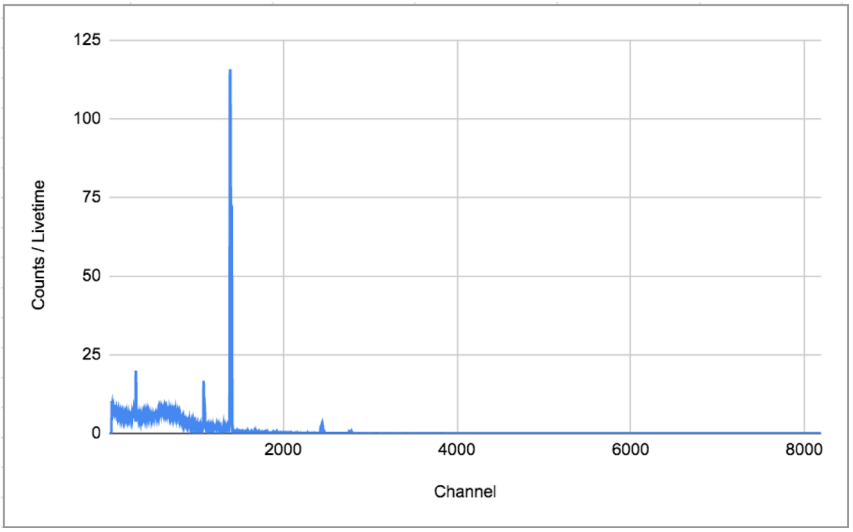

Figure 47: The emitted γ-ray spectrum from charcoal filter cartridge 3 in the passive run.

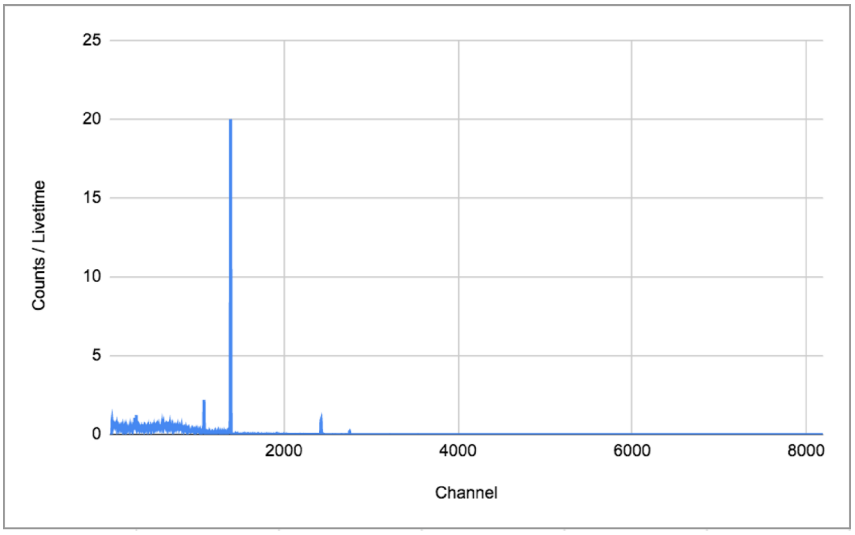

Figure 48: The emitted γ-ray spectrum from charcoal filter cartridge 3 in the passive run when the distance from the detector crystal was increased.

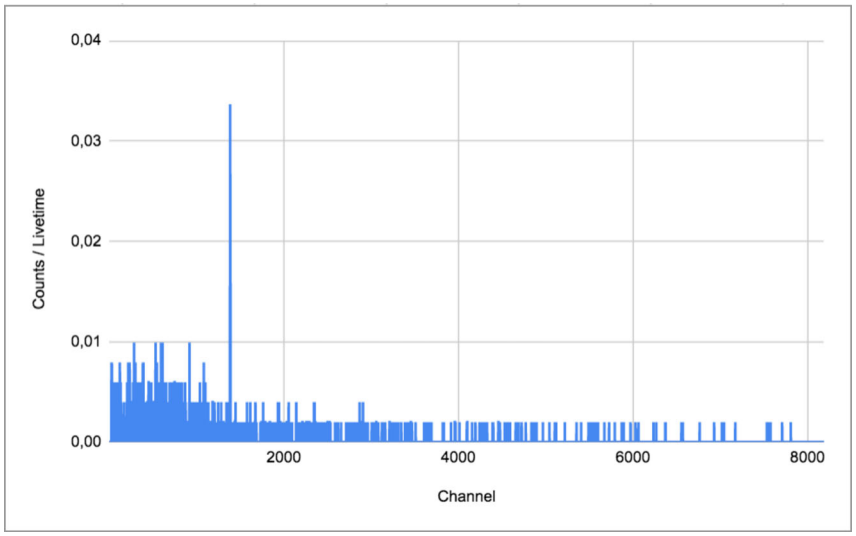

Figure 49: The emitted γ-ray spectrum from the copper filter cartridge from run 1 of the active $CH_3^{131}I$-sampling experiments.

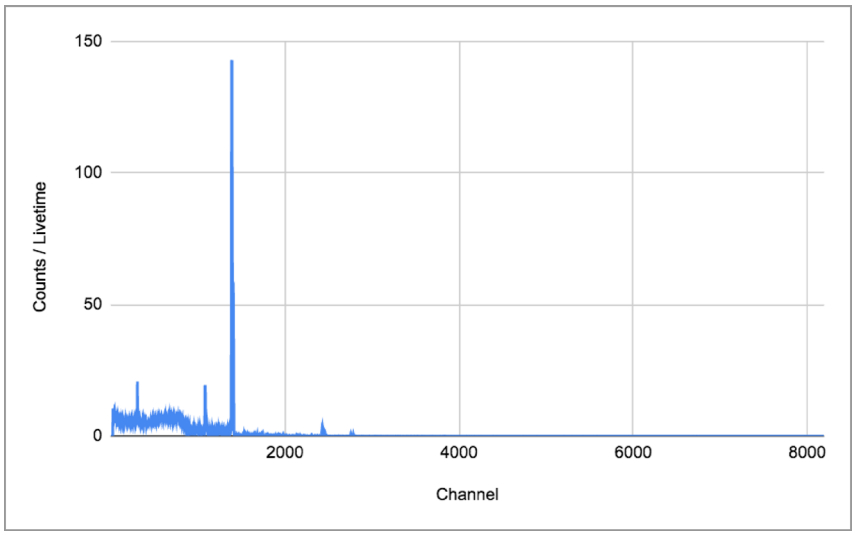

Figure 50: The emitted γ-ray spectrum from charcoal filter cartridge 1 from run 1 of the active $CH_3^{131}I$-sampling experiments.

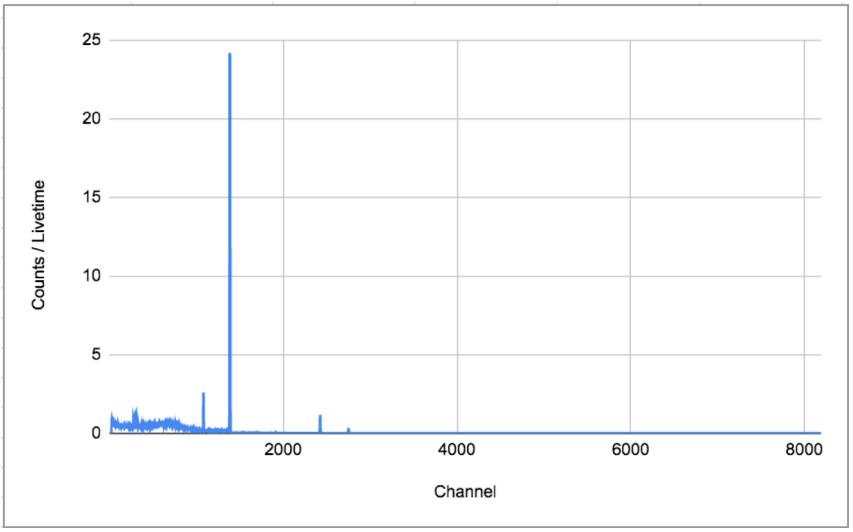

Figure 51: The emitted γ-ray spectrum from charcoal filter cartridge 1 from run 1 of the active $CH_3^{131}I$-sampling experiments when the distance from the detector crystal was increased.

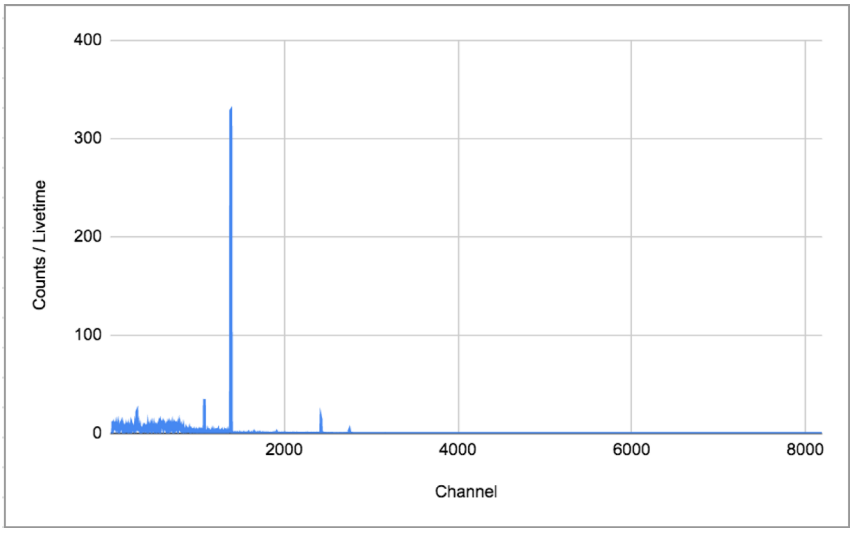

Figure 52: The emitted γ-ray spectrum from charcoal filter cartridge 2 from run 1 of the active $CH_3^{131}I$-sampling experiments.

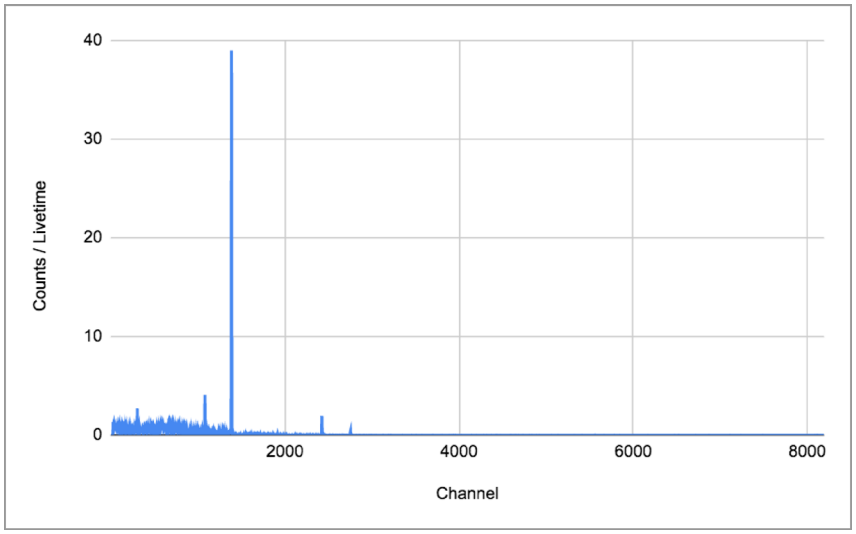

Figure 53: The emitted γ-ray spectrum from charcoal filter cartridge 3 from run 1 of the active $CH_3^{131}I$-sampling experiments.

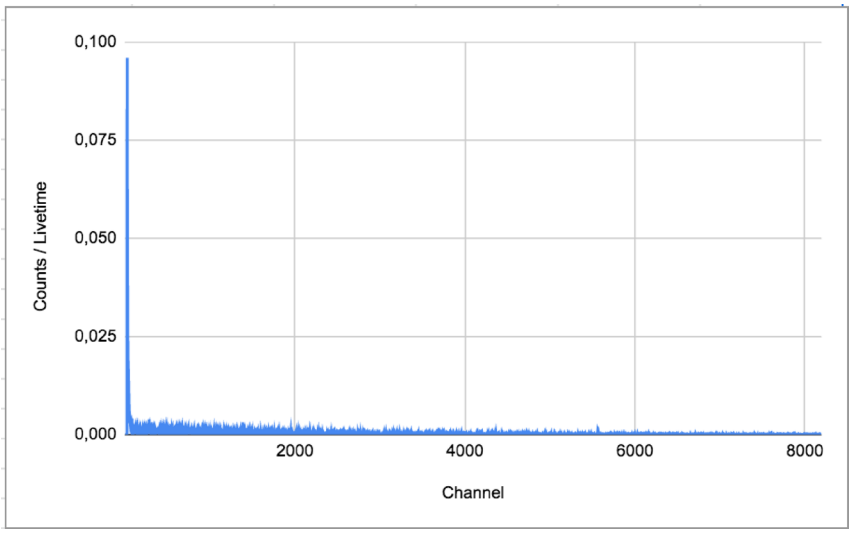

Figure 54: The emitted γ-ray spectrum from charcoal filter cartridge 4 from run 1 of the active $CH_3^{131}I$-sampling experiments.

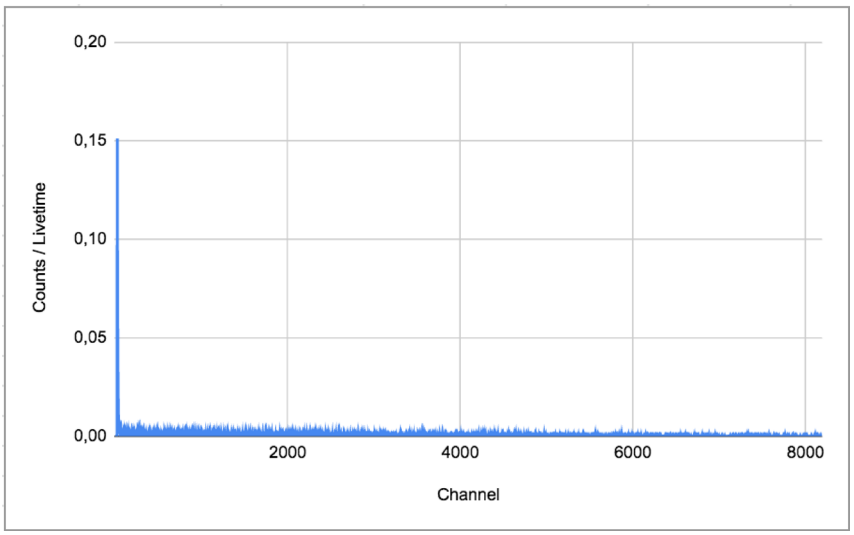

Figure 55: The emitted γ-ray spectrum from charcoal filter cartridge 5 from run 1 of the active $CH_3^{131}I$-sampling experiments.

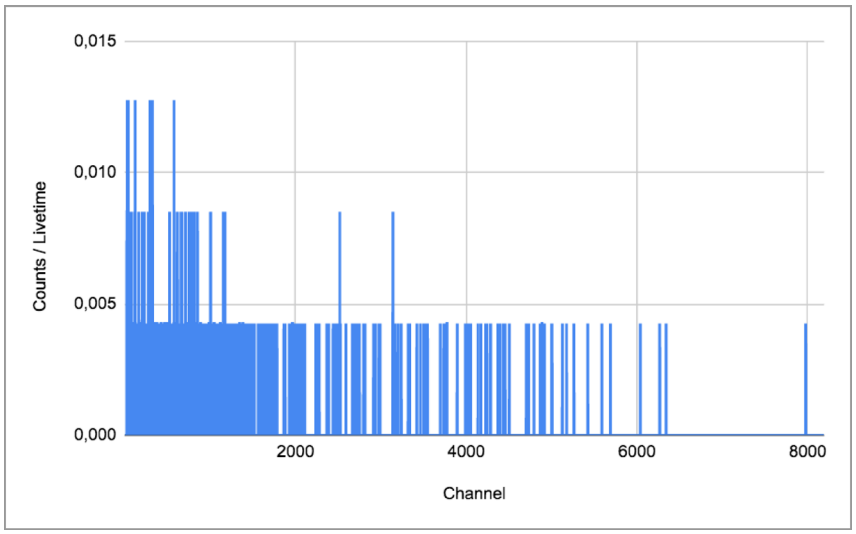

Figure 56: The emitted γ-ray spectrum from the copper filter cartridge from run 2 of the active $CH_3^{131}I$-sampling experiments.

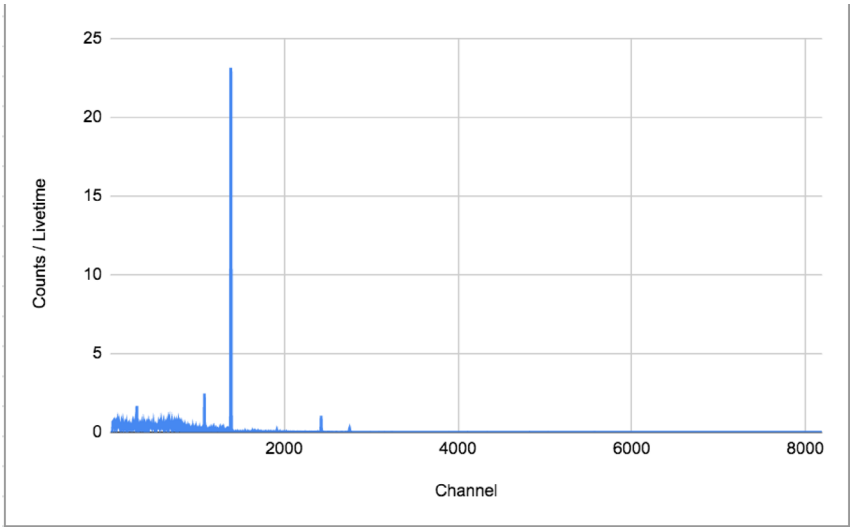

Figure 57: The emitted γ-ray spectrum from charcoal filter cartridge 1 from run 2 of the active $CH_3^{131}I$-sampling experiments.

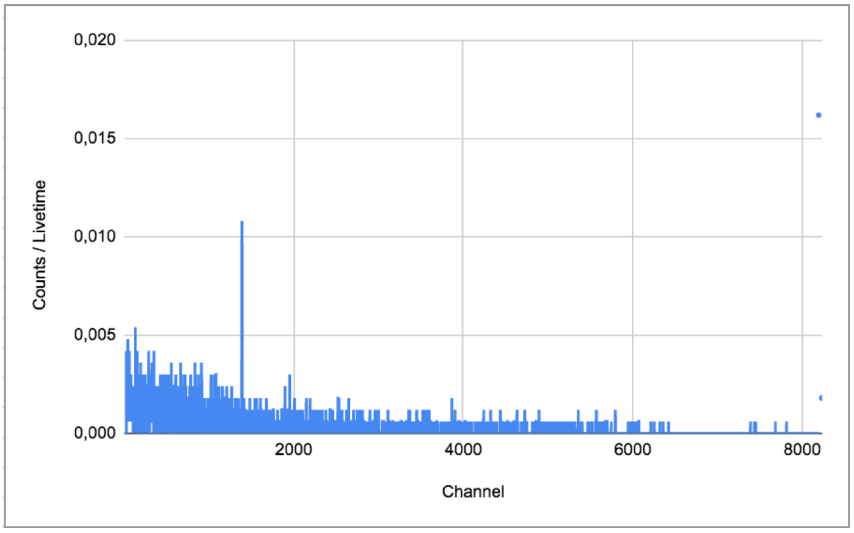

Figure 58: The emitted γ-ray spectrum from charcoal filter cartridge 2 from run 2 of the active $CH_3^{131}I$-sampling experiments.

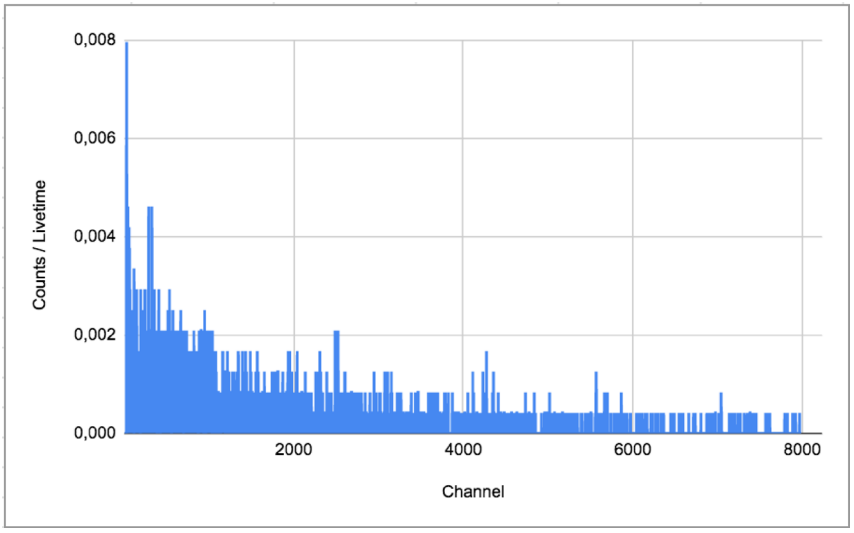

Figure 59: The emitted γ-ray spectrum from charcoal filter cartridge 3 from run 2 of the active $CH_3^{131}I$-sampling experiments.

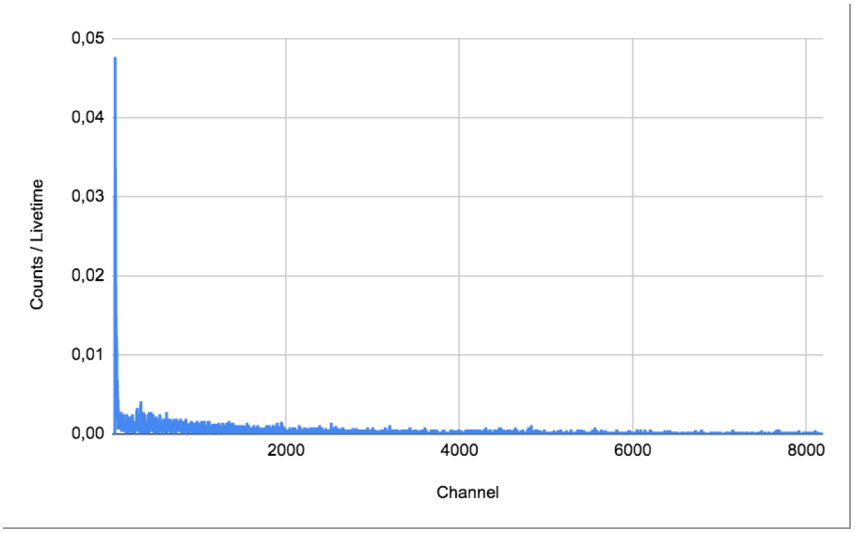

Figure 60: The emitted γ-ray spectrum from charcoal filter cartridge 4 from run 2 of the active $CH_3^{131}I$-sampling experiments.

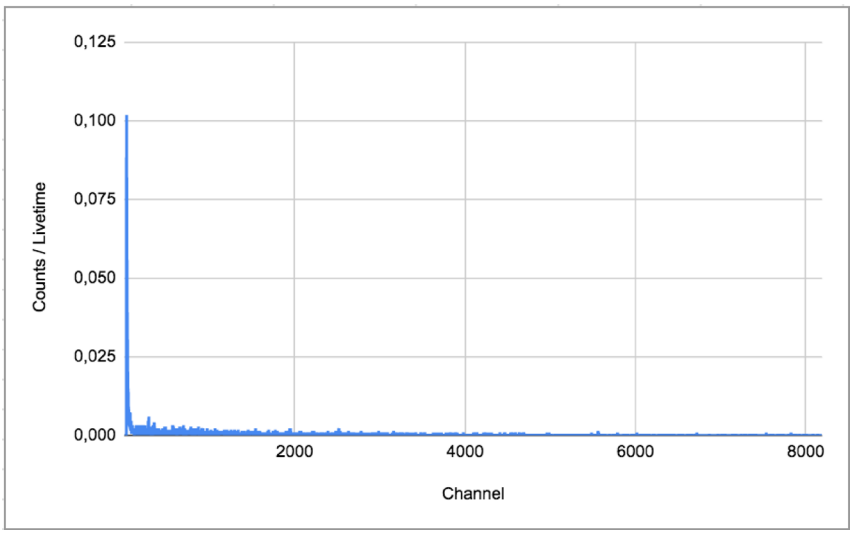

Figure 61: The emitted γ-ray spectrum from charcoal filter cartridge 5 from run 2 of the active $CH_3^{131}I$-sampling experiments.

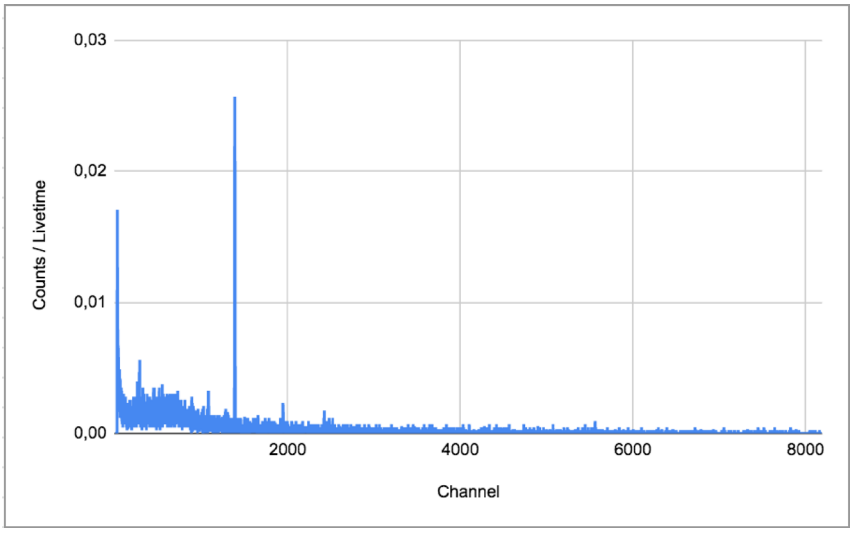

Figure 62: The emitted γ-ray spectrum from the copper filter cartridge from run 3 of the active $CH_3^{131}I$-sampling experiments.

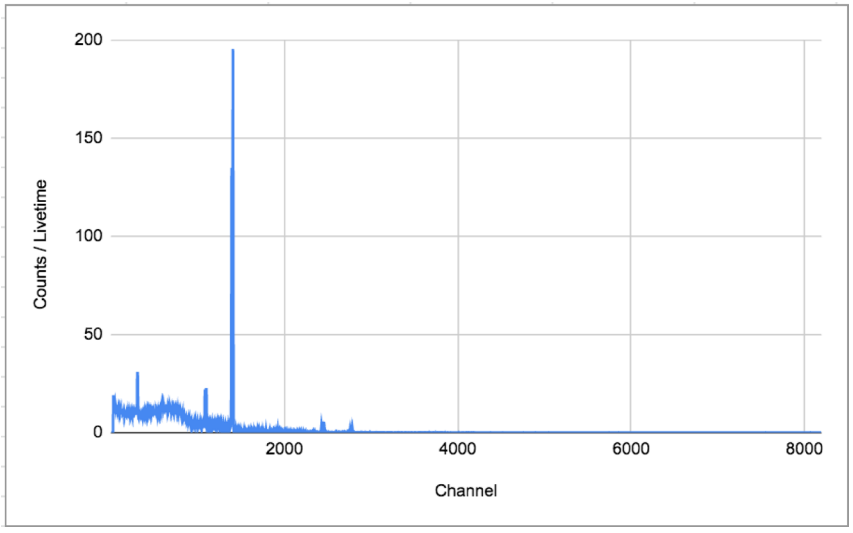

Figure 63: The emitted γ-ray spectrum from charcoal filter cartridge 1 from run 3 of the active $CH_3^{131}I$-sampling experiments.

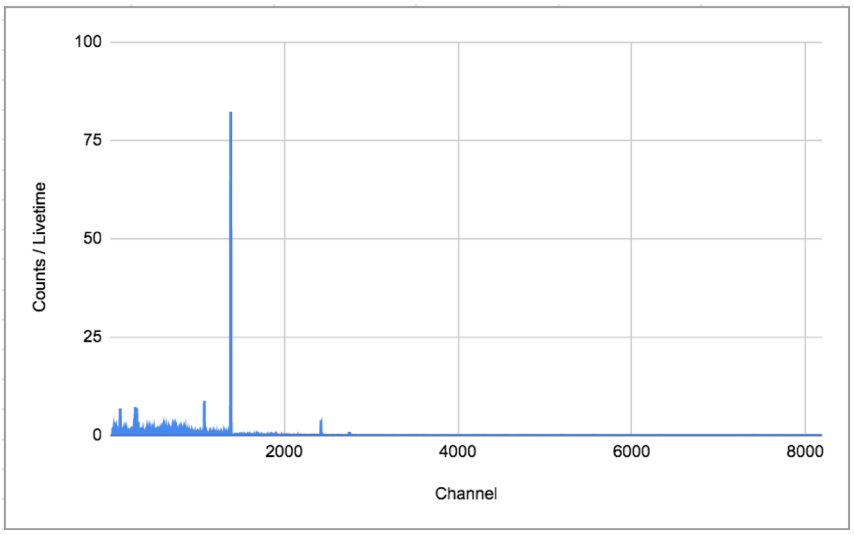

Figure 64: The emitted γ-ray spectrum from charcoal filter cartridge 2 from run 3 of the active $CH_3^{131}I$-sampling experiments when the distance from the detector crystal was increased.

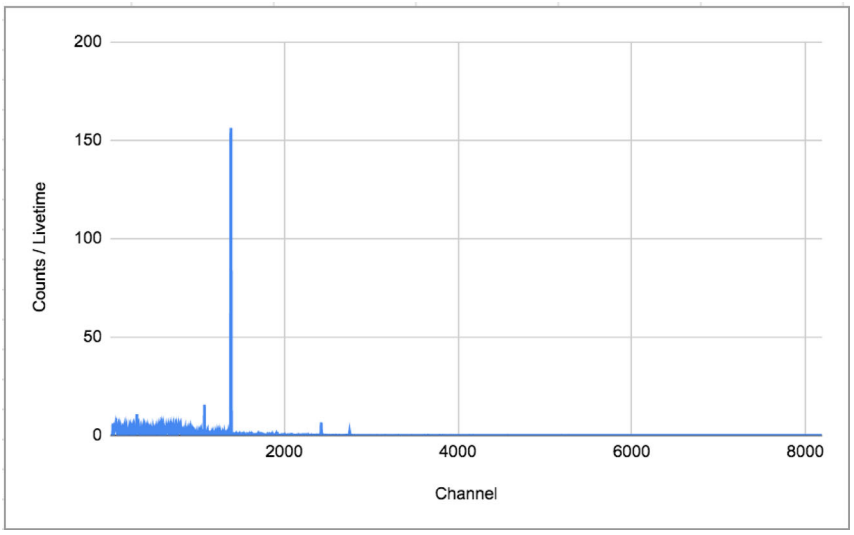

Figure 65: The emitted γ-ray spectrum from charcoal filter cartridge 2 from run 3 of the active $CH_3^{131}I$-sampling experiments.

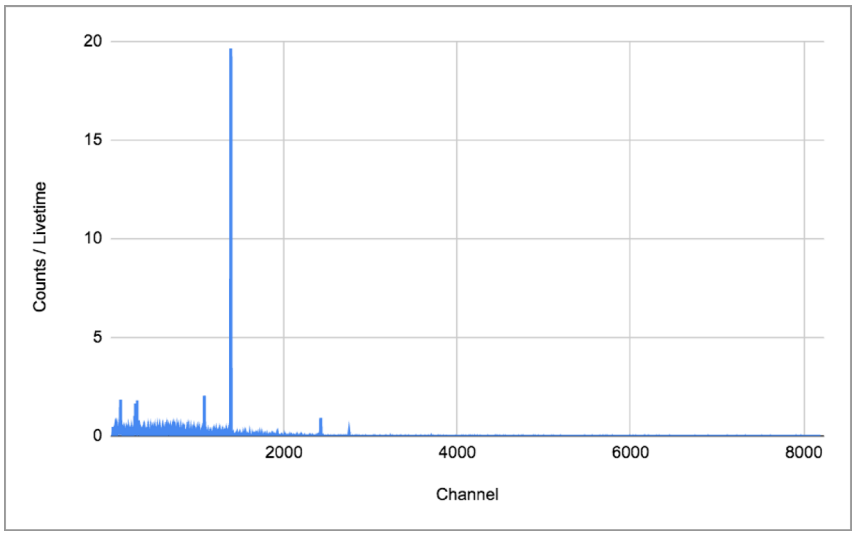

Figure 66: The emitted γ-ray spectrum from charcoal filter cartridge 2 from run 3 of the active $CH_3^{131}I$-sampling experiments when the distance from the detector crystal was increased.

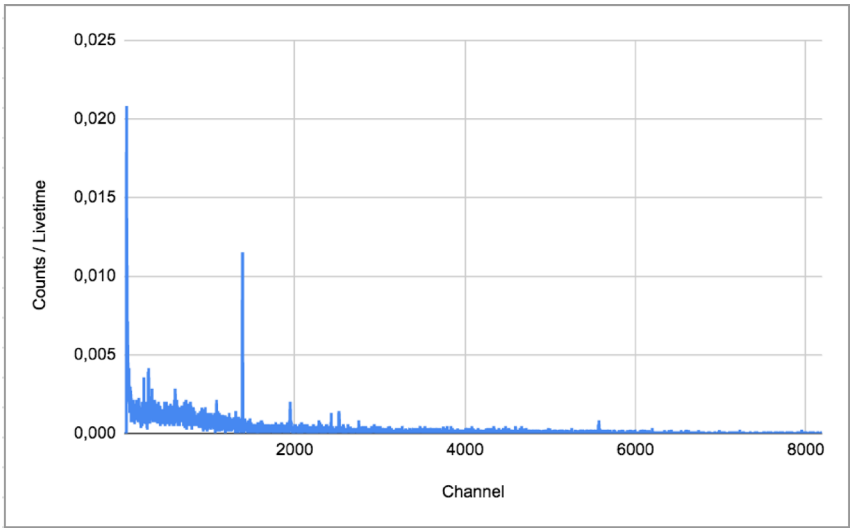

Figure 67: The emitted γ-ray spectrum from charcoal filter cartridge 3 from run 3 of the active $CH_3^{131}I$-sampling experiments.

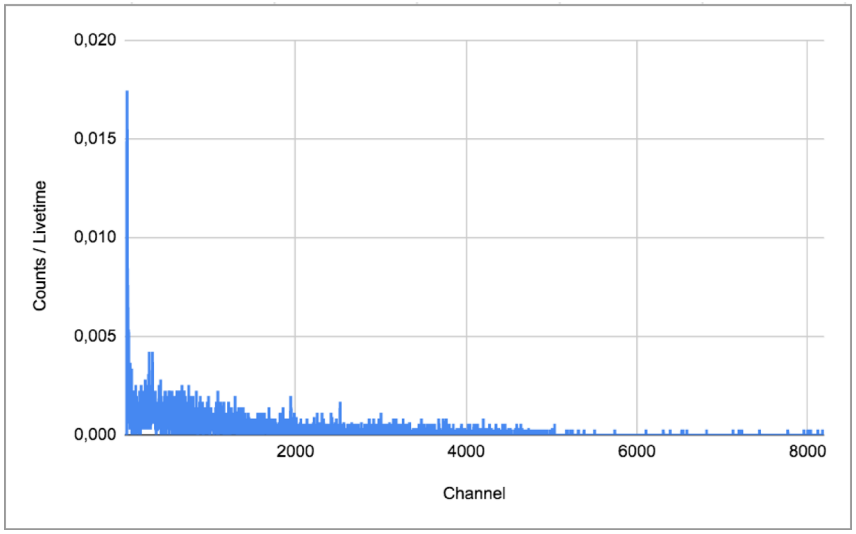

Figure 68: The emitted γ-ray spectrum from charcoal filter cartridge 4 from run 3 of the active $CH_3^{131}I$-sampling experiments.

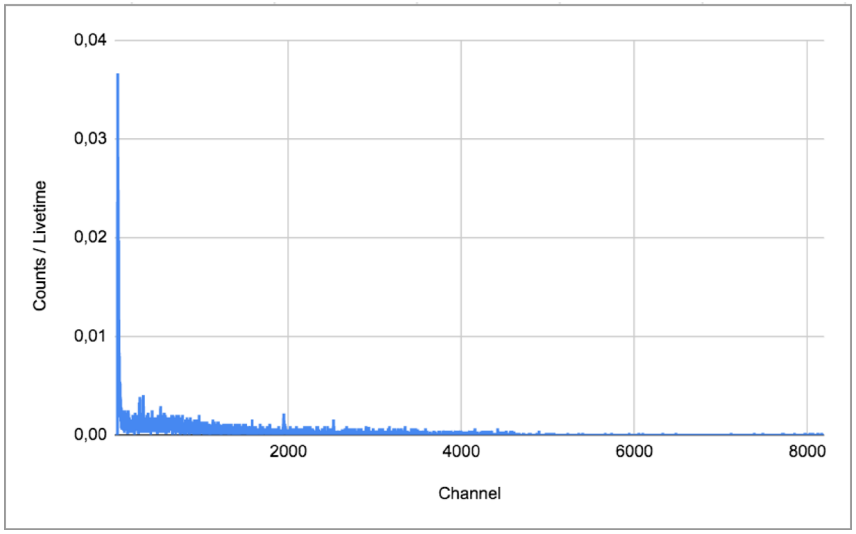

Figure 69: The emitted γ-ray spectrum from charcoal filter cartridge 5 from run 3 of the active $CH_3^{131}I$-sampling experiments.

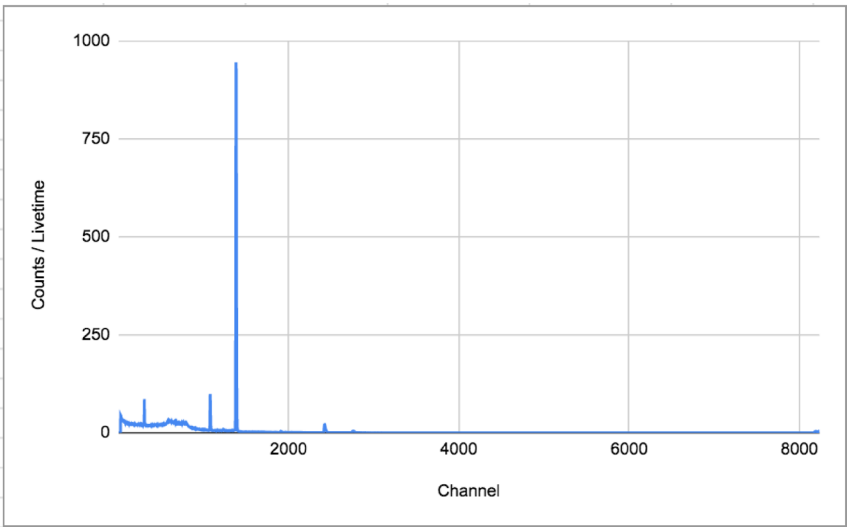

Figure 70: The emitted γ-ray spectrum from charcoal filter cartridge 1 from run 4 of the active $CH_3^{131}I$-sampling experiments.

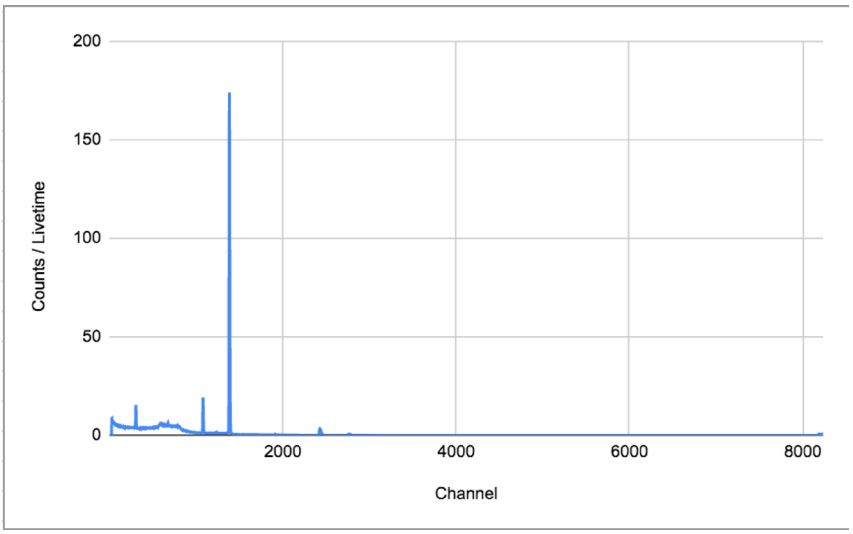

Figure 71: The emitted γ-ray spectrum from charcoal filter cartridge 1 from run 4 of the active $CH_3^{131}I$-sampling experiments when the distance from the detector crystal was increased.

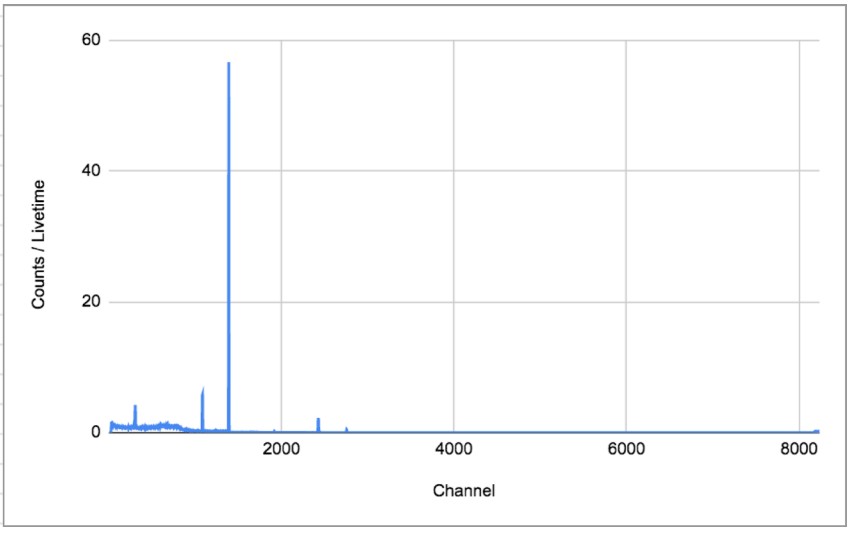

Figure 72: The emitted γ-ray spectrum from charcoal filter cartridge 2 from run 4 of the active $CH_3^{131}I$-sampling experiments.

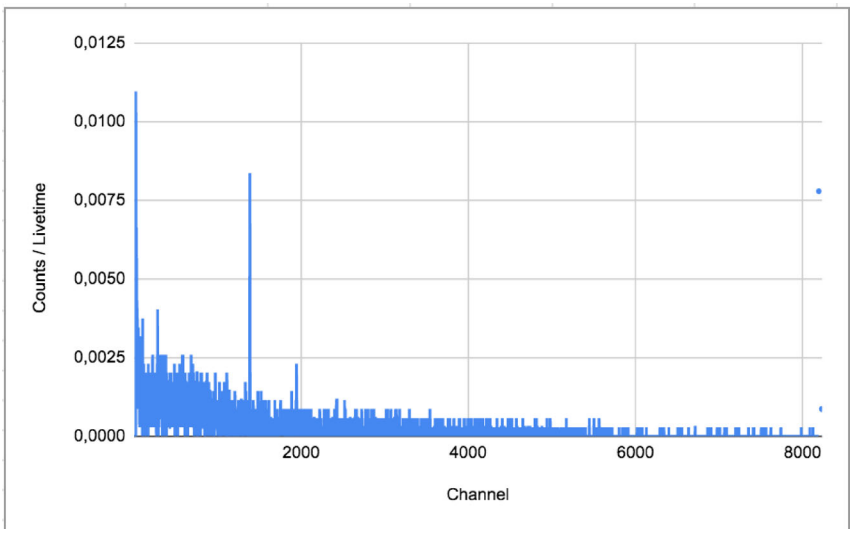

Figure 73: The emitted γ-ray spectrum from charcoal filter cartridge 3 from run 4 of the active $CH_3^{131}I$-sampling experiments.

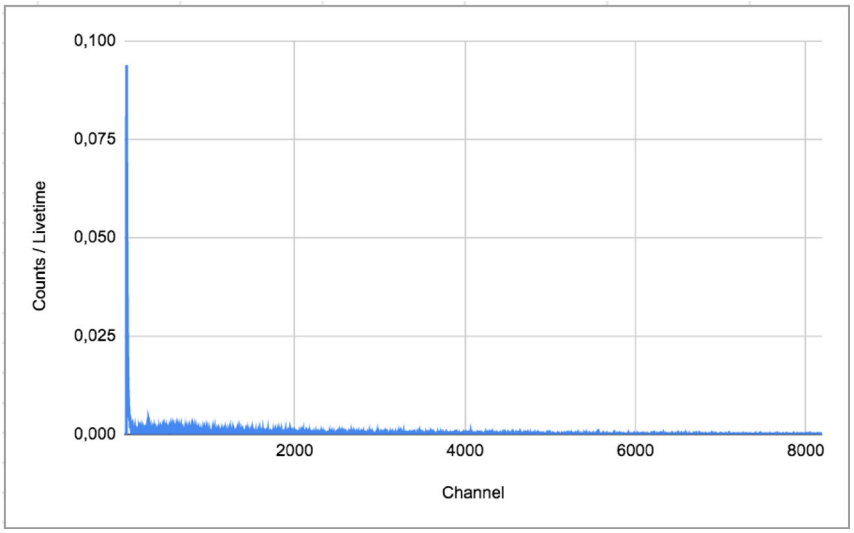

Figure 74: The emitted γ-ray spectrum from charcoal filter cartridge 4 from run 4 of the active $CH_3^{131}I$-sampling experiments.

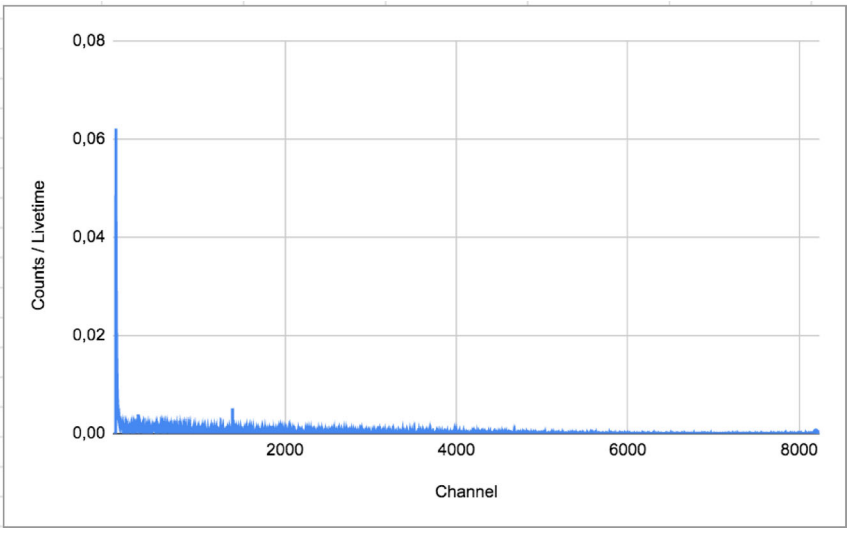

Figure 75: The emitted γ-ray spectrum from charcoal filter cartridge 5 from run 4 of the active $CH_3^{131}I$-sampling experiments.

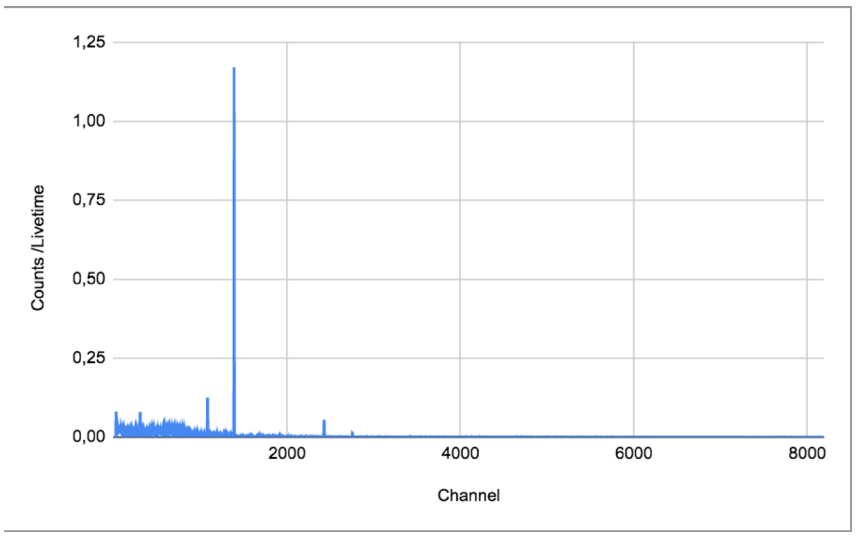

Figure 76: The emitted γ-ray spectrum from the copper filter cartridge from run 5 of the active $CH_3^{131}I$-sampling experiments.

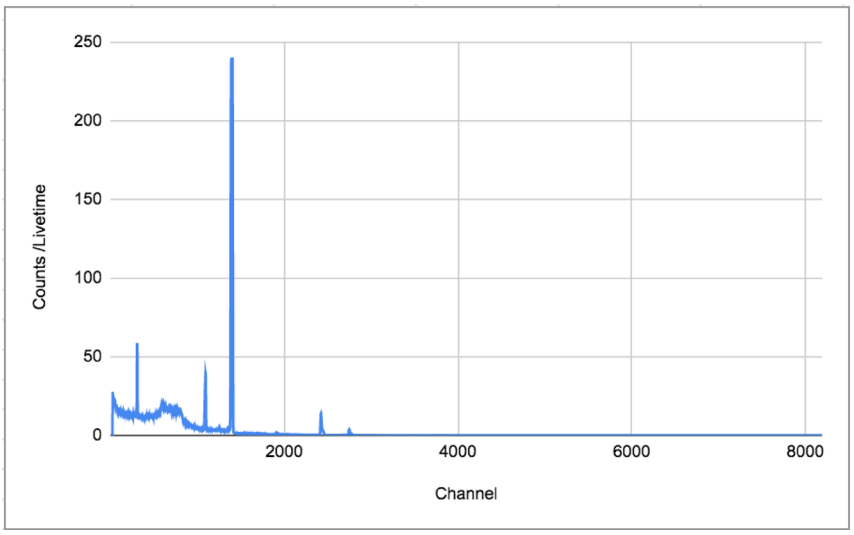

Figure 77: The emitted γ-ray spectrum from the copper filter cartridge 1 from run 5 of the active $CH_3^{131}I$-sampling experiments.

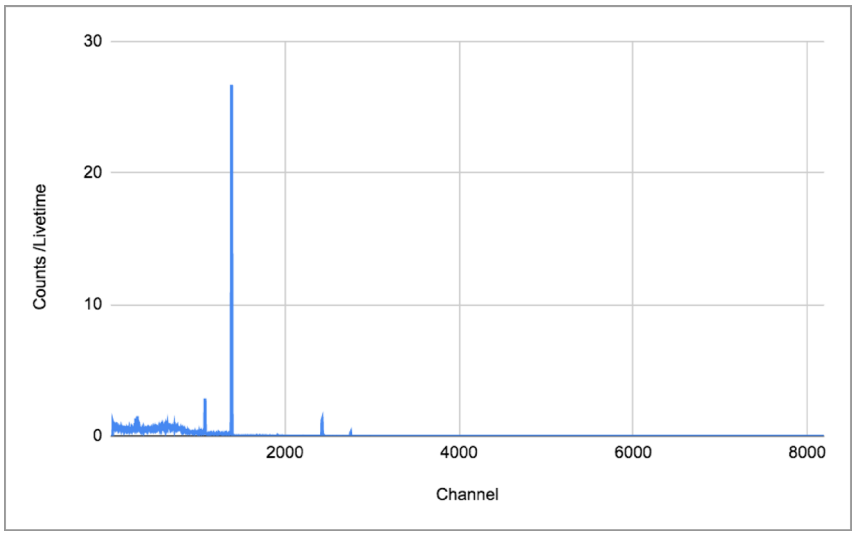

Figure 78: The emitted γ-ray spectrum from charcoal filter cartridge 1 from run 5 of the active $CH_3^{131}I$-sampling experiments when the distance from the detector crystal was increased.

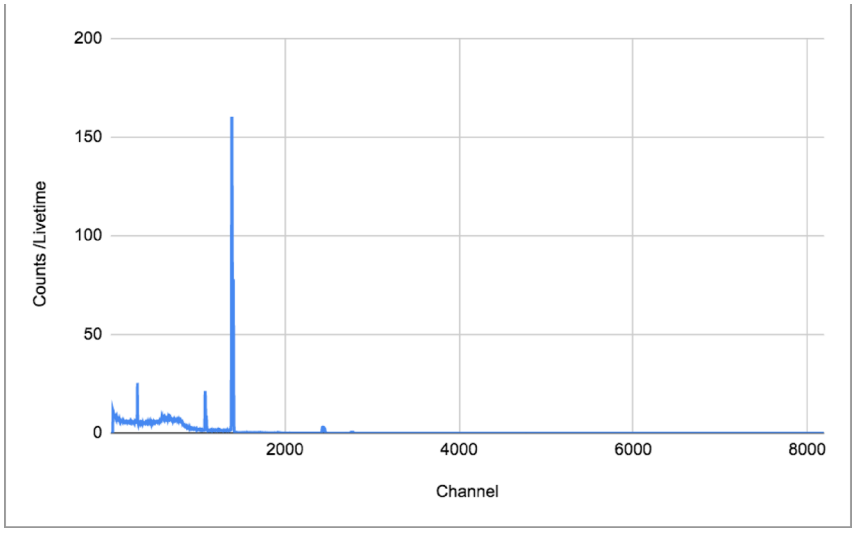

Figure 79: The emitted γ-ray spectrum from the copper filter cartridge 2 from run 5 of the active $CH_3^{131}I$-sampling experiments.

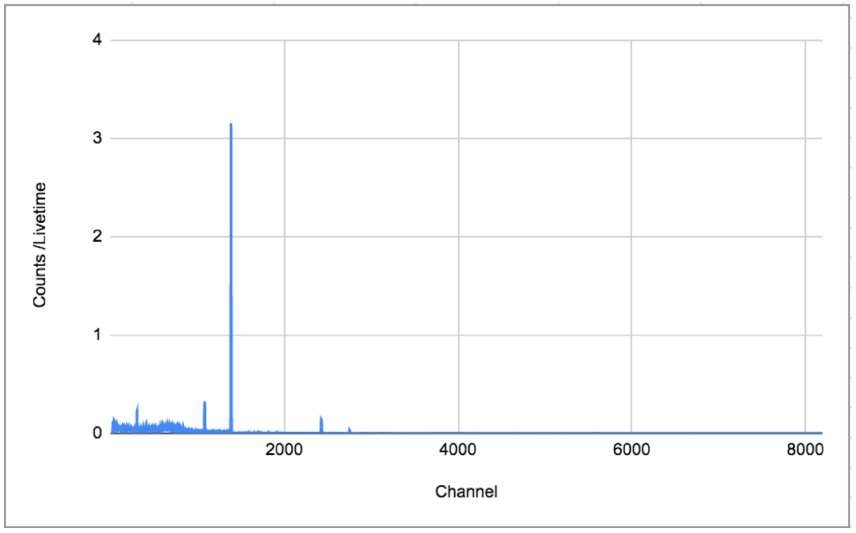

Figure 80: The emitted γ-ray spectrum from the copper filter cartridge 3 from run 5 of the active $CH_3^{131}I$-sampling experiments.

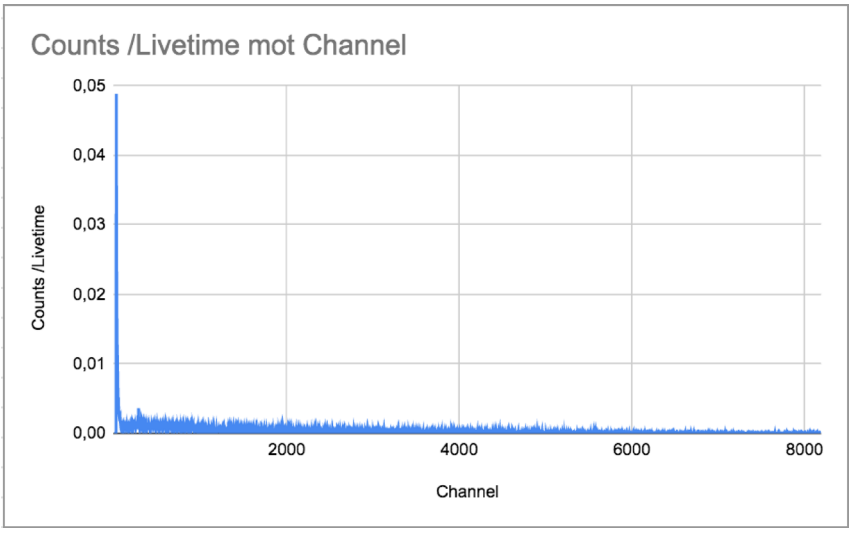

Figure 81: The emitted γ-ray spectrum from the copper filter cartridge 4 from run 5 of the active $CH_3^{131}I$-sampling experiments.

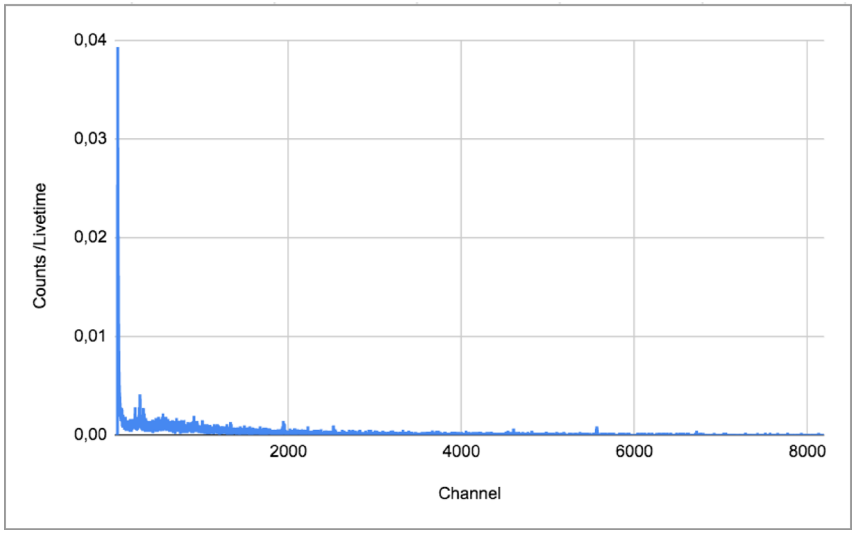

Figure 82: The emitted γ-ray spectrum from the copper filter cartridge 5 from run 5 of the active $CH_3^{131}I$-sampling experiments.

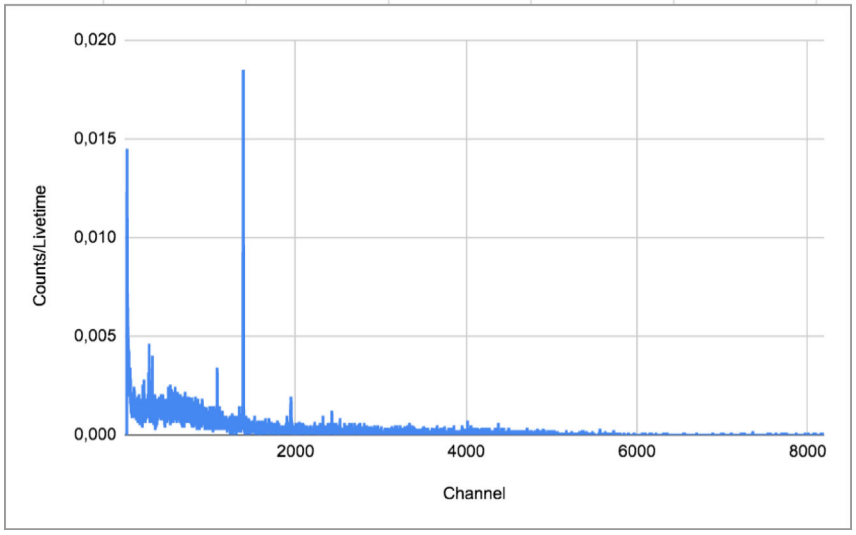

Figure 83: The emitted γ-ray spectrum from the copper filter cartridge from run 6 of the active $CH_3^{131}I$-sampling experiments.

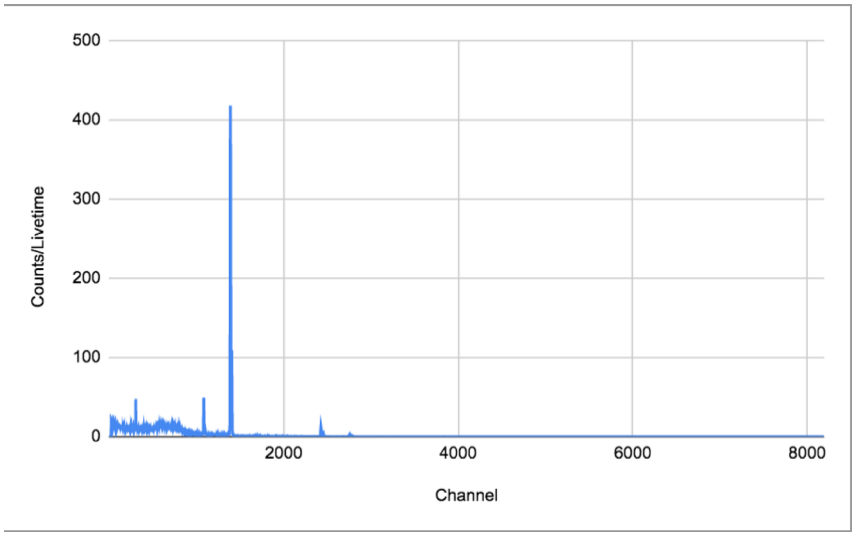

Figure 84: The emitted γ-ray spectrum from the copper filter cartridge 1 from run 6 of the active $CH_3^{131}I$-sampling experiments.

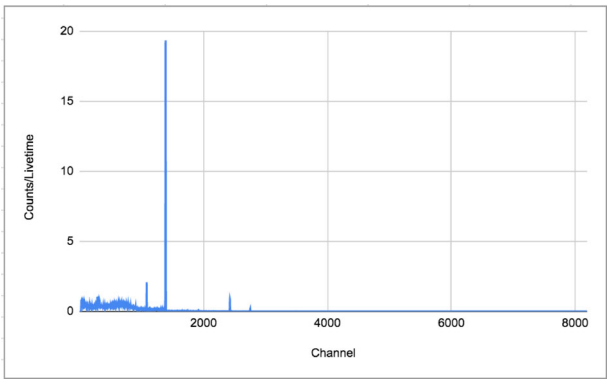

Figure 85: The emitted γ-ray spectrum from the copper filter cartridge 1 from run 6 of the active $CH_3^{131}I$-sampling experiments when the distance from the detector crystal was increased.

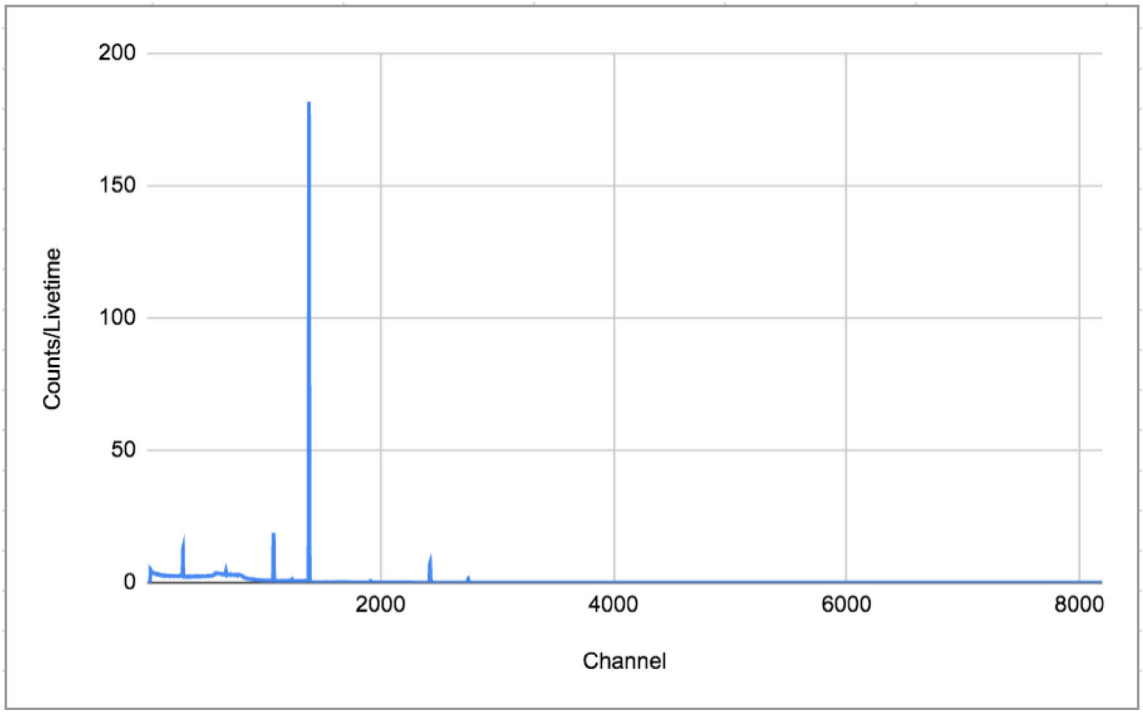

Figure 86: The emitted γ-ray spectrum from the copper filter cartridge 2 from run 6 of the active $CH_3^{131}I$-sampling experiments.

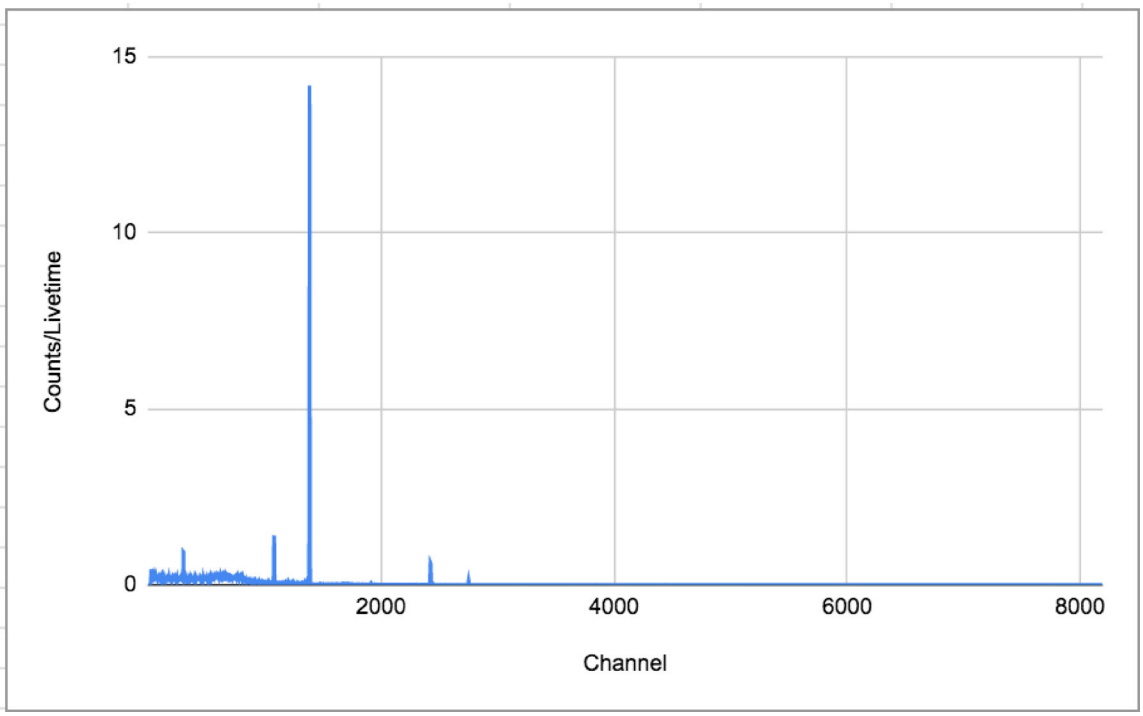

Figure 87: The emitted γ-ray spectrum from the copper filter cartridge 3 from run 6 of the active $CH_3^{131}I$-sampling experiments.

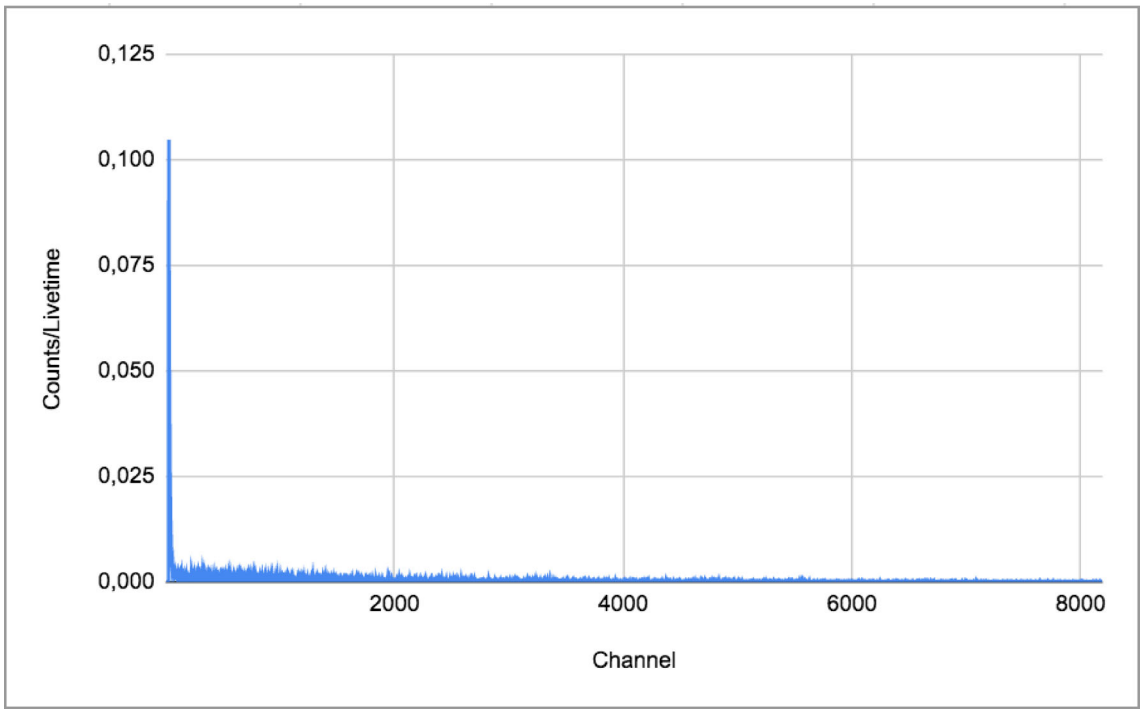

Figure 88: The emitted γ-ray spectrum from the copper filter cartridge 4 from run 6 of the active $CH_3^{131}I$-sampling experiments.

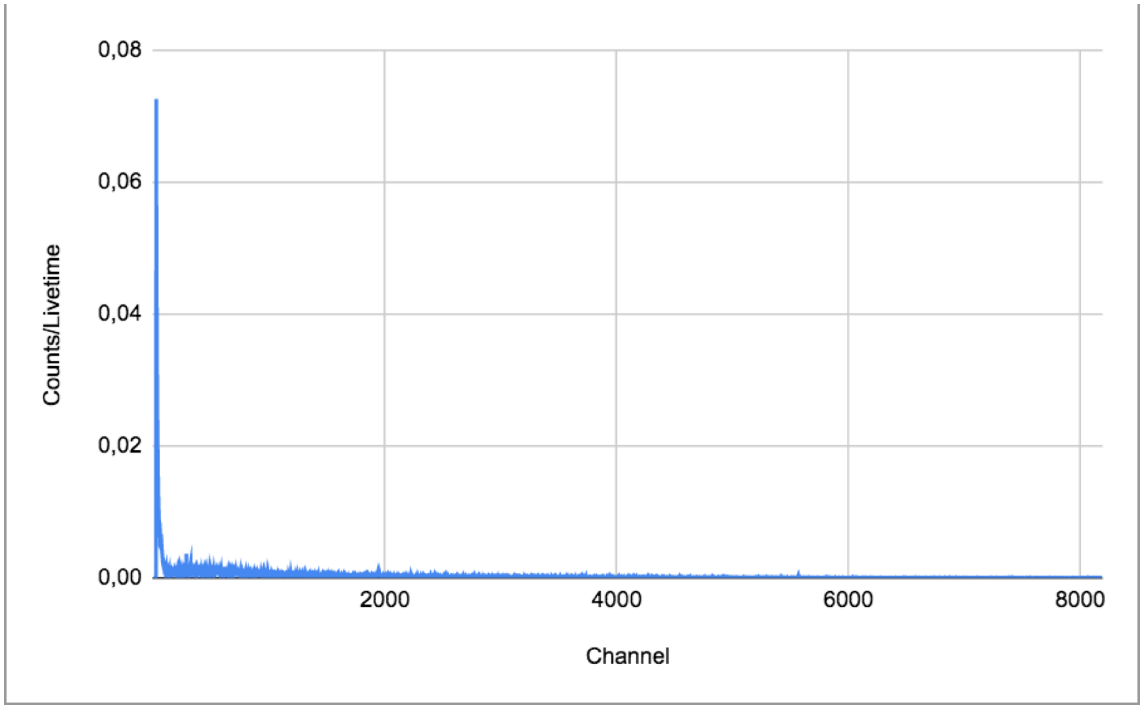

Figure 89: The emitted γ-ray spectrum from the copper filter cartridge 5 from run 6 of the active $CH_3^{131}I$-sampling experiments.